JOURNAL OF GEOPHYSICAL RESEARCH: ATMOSPHERES, VOL. 118, 1–17, doi:10.1029/2012JD018327, 2013

Hydrocarbons in the upper troposphere and lower stratosphere observed from ACE-FTS and comparisons with WACCM

Mijeong Park,[1] William J. Randel,[1] Douglas E. Kinnison,[1] Louisa K. Emmons,[1] Peter F. Bernath,[2] Kaley A. Walker,[3] Chris D. Boone,[4] and Nathaniel J. Livesey[5]

Received 19 June 2012; revised 28 November 2012; accepted 29 November 2012.

[1] Satellite measurements from the Atmospheric Chemistry Experiment Fourier Transform Spectrometer (ACE-FTS) are used to examine the global, seasonal variations of several hydrocarbons, including carbon monoxide (CO), ethane (C_2H_6), acetylene (C_2H_2), and hydrogen cyanide (HCN). We focus on quantifying large-scale seasonal behavior from the middle troposphere to the stratosphere, particularly in the tropics, and furthermore make detailed comparisons with the Whole Atmosphere Community Climate Model (WACCM) chemistry climate model (incorporating tropospheric photochemistry, time-varying hydrocarbon emissions, and meteorological fields nudged from reanalysis). Comparisons with Microwave Limb Sounder (MLS) measurements of CO are also included to understand sampling limitations of the ACE-FTS data and biases among observational data sets. Results show similar overall variability for CO, C_2H_6, and C_2H_2, with a semiannual cycle in the tropical upper troposphere related to seasonallyvarying sources and deep tropical convection, plus a maximum during Northern Hemisphere summer tied to the Asian monsoon anticyclone. These species also reveal a strong annual cycle above the tropical tropopause, tied to annual variations in the upward branch of Brewer-Dobson circulation. HCN reveals substantial differences from the other species, due to a longer photochemical lifetime and a chemical sink associated with ocean surface contact, which produces a minimum in the tropical upper troposphere not observed in the other species. For HCN, transport to the stratosphere occurs primarily through the Asian summer monsoon anticyclone. Overall, the WACCM simulation is able to reproduce most of the large-scale features observed in the ACE-FTS data, suggesting a reasonable simulation of sources and large-scale transport. The model is too low in the Southern Hemisphere subtropics during Austral spring, which indicates underestimate of biomass burning emissions and/or insufficient vertical transport in the model.

Citation: Park, M., W. J. Randel, D. E. Kinnison, L. K. Emmons, P. F. Bernath, K. A. Walker, C. D. Boone, and N. J. Livesey (2013), Hydrocarbons in the upper troposphere and lower stratosphere observed from ACE-FTS and comparisons with WACCM, *J. Geophys. Res. Atmos.*, *118*, doi:10.1029/2012JD018327.

1. Introduction

[2] Hydrocarbons are key components of tropospheric chemical cycles, of relevance for ozone and aerosols and their precursors, and they contribute to determining the oxidizing capacity of the atmosphere. Tropospheric hydrocarbons originate from combustion (fossil fuel and biomass burning), along with biogenic and ocean sources, and the primary loss mechanisms are linked to photolysis and reactions with the hydroxyl radical (OH). Hydrocarbons have typical photochemical lifetimes of hours to several months and can provide information regarding transport and circulation throughout the troposphere [e.g., *Bowman*, 2006]. While measurements of hydrocarbons have historically been obtained from surface, balloon, or aircraft measurements [*Rudolph*, 1995; *Schneider et al.*, 1997; *Rinsland et al.*, 1998; *Zhao et al.*, 2002; *Russo et al.*, 2003; *Singh et al.*, 2003; *Baker et al.*, 2011], new information is becoming available from satellite observations [e.g., *Pumphrey et al.*, 2008; *Funke et al.*, 2009; *Glatthor et al.*, 2009; *Wiegele et al.*, 2012] to map their global behavior. Such data are especially useful for comprehensive comparisons with global chemical transport model (CTM) simulations [*Duncan et al.*, 2007; *Barret et al.*, 2008; *Turquety et al.*, 2008; *Lupu et al.*, 2009; *Liu et al.*, 2010; *González Abad et al.*, 2011].

[1]National Center for Atmospheric Research, Boulder, Colorado, USA.
[2]Department of Chemistry and Biochemistry, Old Dominion University, Norfolk, Virginia, USA.
[3]Department of Physics, University of Toronto, Toronto, Ontario, Canada.
[4]Department of Chemistry, University of Waterloo, Waterloo, Ontario, Canada.
[5]Jet Propulsion Laboratory, California Institute of Technology, Pasadena, California, USA.

Corresponding author: M. Park, National Center for Atmospheric Research, PO Box 3000, Boulder, CO 80307, USA. (mijeong@ucar.edu)

2169-897X/13/2012JD018327

[3] The focus of this study is a systematic evaluation of the global climatological behavior of several hydrocarbons measured by the Atmospheric Chemistry Experiment Fourier Transform Spectrometer (ACE-FTS) satellite instrument, accompanied by detailed comparisons with a current generation chemistry climate model. The simulations are based on the Whole Atmosphere Community Climate Model (WACCM) [*Garcia et al*., 2007], incorporating a comprehensive tropospheric chemistry mechanism, time-varying surface emissions, and meteorological fields nudged from reanalysis data (described in detail below). Our analyses focus on carbon monoxide (CO), ethane (C_2H_6), acetylene (C_2H_2), and hydrogen cyanide (HCN). Although CO is not technically a hydrocarbon, it behaves in a manner similar to many other hydrocarbons (with similar sources and sinks), and has also been extensively studied in previous work [e.g., *Rinsland et al*., 1998, 2005; *Clerbaux et al*., 2005, 2008; *Park et al*., 2007, 2009; *Turquety et al*., 2008; *George et al*., 2009]. CO is somewhat distinct from the other species in that approximately one-half of the tropospheric burden originates from in situ photochemical production (from oxidation of methane and more complex hydrocarbons), whereas surface emissions are the main sources for C_2H_6, C_2H_2, and HCN. The ACE-FTS provides measurements spanning the middle troposphere to the mesosphere (with vertical resolution of ~3 km), and we focus here on the altitude region ~5–30 km. Note that CO and other hydrocarbons can be especially useful tracers for understanding transport near the tropopause, often used in combination with ozone [*Pan et al*., 2004; *Hegglin et al*., 2009]. We furthermore include comparisons of CO observations between ACE-FTS and the Aura Microwave Limb Sounder (MLS) instrument, which has more extensive space-time sampling (but limited to higher altitudes in the troposphere) than ACE-FTS.

[4] There have been a number of observational studies of global tropospheric CO behavior based on satellite measurements, including data from the Measurement of Pollution in the Troposphere (MOPITT) instrument [*Edwards et al*., 2004, 2006] on the Terra spacecraft, Scanning Imaging Absorption Spectrometer for Atmospheric Cartography (SCIAMACHY) onboard the Envisat satellite [*de Laat et al*., 2006; *Kopacz et al*., 2010], and Infrared Atmospheric Sounding Interferometer (IASI) on board MetOp-A [*George et al*., 2009; *Turquety et al*., 2009]. These instruments primarily measure relatively broad vertical layers of tropospheric CO. The Tropospheric Emission Spectrometer (TES) onboard the Aura satellite [*Beer*, 2006] provides CO profiles and column amount in the troposphere [*Luo et al*., 2007]. The Michelson Interferometer for Passive Atmospheric Sounding (MIPAS) is a midinfrared Fourier transform limb emission spectrometer on Envisat, which provides vertically resolved CO mixing ratios from upper troposphere to mesosphere [*Fischer et al*., 2008]. *Funke et al*. [2009] presented detailed distributions of MIPAS CO in the stratosphere and mesosphere from observations covering September 2003 to March 2004, highlighting stratospheric seasonal variations over high latitudes and enhanced CO plumes in the upper troposphere. MLS measures vertical profiles of CO in the upper troposphere and stratosphere, and the long record of global MLS measurements (2004–2013) has provided information on variability across a broad range of scales [e.g., *Liu et al*., 2007; *Liu et al*, 2010; *Abalos et al*., 2012].

[5] Observations of enhanced tropospheric hydrocarbons in biomass burning plumes have been reported from various satellite data, including ACE-FTS CO [*Rinsland et al*., 2005, 2007; *Dufour et al*., 2006; *Coheur et al*., 2007; *Tereszchuk et al*., 2011], C_2H_6 from ACE-FTS [*Rinsland et al*., 2005, 2007] and MIPAS [*von Clarmann et al*., 2007; *Glatthor et al*., 2009; *Wiegele et al*., 2012], and C_2H_2 and HCN from ACE-FTS [*Rinsland et al*., 2005] and MIPAS [*Glatthor et al*., 2009; *Parker et al*., 2011; *Wiegele et al*., 2012]. These observations focus on limited geographic regions and specific events. *González Abad et al*. [2011] showed that the GEOS-Chem CTM is able to reproduce the seasonal cycles of CO and C_2H_6 (derived from ACE-FTS) reasonably well, but underestimates concentrations in the Northern Hemisphere. Comparison between ACE-FTS HCN and the Global Environmental Multiscale Air Quality model (GEM-AQ) shows reasonable agreement for seasonal variations in the upper troposphere [*Lupu et al*., 2009]. Interannual variations of HCN in the lower stratosphere have been studied by *Pumphrey et al*. [2008], *Li et al*. [2009], and *Pommrich et al*. [2010]. *De Smedt et al*. [2010] reported trends in tropospheric formaldehyde columns retrieved from GOME and SCIAMACHY observations between 1997 and 2009, which they attribute to changes in anthropogenic emissions.

[6] The novel contribution of this paper is the systematic development of a global seasonally varying climatology of hydrocarbons derived from over seven years of global ACE-FTS observations, and using these results to evaluate a current generation troposphere-stratosphere CTM. We include over 21,000 ACE-FTS occultation measurements to construct three-dimensional seasonal climatologies covering the middle troposphere to middle stratosphere, with vertical resolution of ~3 km. We compare and contrast the global behaviors of CO, C_2H_6, C_2H_2, and HCN (which have different lifetimes, sources, and sinks) to provide information regarding seasonal variations in circulation and transport in the UTLS. The model comparisons are beneficial for evaluating emission inventories and model transport behavior, and the ACE-FTS climatologies can serve as a benchmark for constraining comprehensive tropospheric chemistry simulations. The ACE-FTS climatologies derived and analyzed here are freely available as supplementary material to this paper (http://www.ace.uwaterloo.ca/) for similar analysis by the wider community.

2. Data and Model Description

2.1. Satellite Data

[7] The Atmospheric Chemistry Experiment (ACE) is a satellite mission onboard the Canadian science satellite, SCISAT-1, which was launched into a high inclination (74°) and low earth orbit (650 km) on 12 August 2003 [*Bernath et al*., 2005]. The ACE Fourier Transform Spectrometer (ACE-FTS) is a solar occultation instrument measuring the infrared absorption spectra at high resolution ($0.02\,cm^{-1}$) from 2.4 to 13.3 μm that provides a comprehensive set of trace gas mixing ratios from the lower thermosphere (~5–150 km). The vertical field of view (FOV) of the instrument is ~3 km, with vertical oversampling providing an effective vertical resolution of 2–3 km; the retrievals are performed on a 1 km vertical grid [*Boone et al*., 2005]. We focus on the ACE-FTS measurements of CO, C_2H_6, C_2H_2 and HCN

covering approximately 5 to 30 km in altitude. The data used here are based on retrieval version 3, covering the period from February 2004 to October 2010.

[8] The sampling of ACE-FTS (resulting from the high inclination satellite orbit) provides measurements primarily over high latitudes, with limited sampling through the tropics, four times per year (February, April, August, and October) [see *Bernath*, 2006]. We focus on seasonal averages constructed by combining data into four seasons: December–February (DJF), March–May (MAM), June–August (JJA), and September–November (SON); these data cover much of the globe, but have a limited number of measurements within each season, especially in the tropics. A climatology of gridded data is constructed by combining measurements from all seven years (~21,000 total vertical profiles), gridded onto a 12° latitude × 24° longitude grid using Gaussian-weighted averaging of all measurements within 1000 km of a grid box (with a Gaussian half-width of 500 km). The size of the horizontal grids and the Gaussian half-width are chosen to provide global coverage and resolve regional structures. However, caution should be used for interpreting the gridded maps where the data is sparse, for instance, in the tropical upper troposphere. For data screening purposes, we exclude outliers using three sigma standard deviation from the averages within every 30 degrees latitude between 90°S–90°N (less than 1% of the total profiles). This has little or no impact on zonal averages, but removes spikes in horizontal maps at fixed altitudes.

[9] The total error associated with ACE-FTS CO partial columns is on the order of 0.5%–2% between ~20–50 km, based on the occultations included in the analysis of *Clerbaux et al*. [2008]. Retrievals for C_2H_6 and C_2H_2 span altitudes from ~7 to 20 km. Retrieval errors for C_2H_6 are 15%–25% between 7–12 km and more than 30% above 12 km for the occultations considered in *González Abad et al*. [2011]. C_2H_2 errors are dependent on latitude and altitude (25%–30% in the polar regions, increasing toward the tropics). Retrievals for HCN extend from ~7 to above 30 km [*Rinsland et al*., 2005]. Random error ranges from 5%–10% at 8.5 km and decreases in the lower stratosphere. Systematic error based on the contribution from the spectroscopic constants for HCN ranges from 2%–5% [*Lupu et al*., 2009].

[10] For further comparisons of CO measurements (and to quantify any regional and temporal biases introduced by the ACE-FTS sampling), we also examine CO measurements from the Aura MLS satellite instrument. The Aura MLS [*Waters et al*., 2006] was launched into a Sun-synchronous near-circular polar orbit on 15 July 2004; MLS provides daily global coverage from 82°S–82°N consisting of approximately 14 orbits per day. We use MLS CO level 2 products based on version 3.3 (v3.3) retrieval algorithms covering the period August 2004 to December 2010 [*Livesey et al*., 2011], reported on fixed pressure levels (215, 147, 100, 68, 46 hPa, etc.). The vertical resolution of MLS CO is approximately 4.5 km in the UTLS region, somewhat coarser than ACE-FTS. Systematic uncertainty in MLS CO is about ±20 ppbv (±30%) at 100 hPa and ±30 ppbv (±30%) at 147 hPa [*Livesey et al*., 2008]. A factor of two high bias at 215 hPa in the previous version of MLS CO retrievals has been eliminated in v3.3. We construct gridded MLS CO data on 5° latitude × 10° longitude grids [as in *Park et al*., 2009] on each day, and individual profiles are quality screened per *Livesey et al*. [2011]. Seasonal averages of MLS CO are constructed from the monthly averages from 2004 to 2010.

[11] We use temperature from the National Centers for Environmental Prediction/National Center for Atmospheric Research (NCEP/NCAR) reanalysis [*Kistler et al*., 2001] covering the period 2004 to 2010 to calculate isentropes and the thermal tropopause in conjunction with MLS and ACE-FTS chemical constituents data. For the WACCM results, tropopause and isentropes are derived using WACCM temperatures. In order to examine relationships with climatological deep convection, we include statistics of monthly interpolated outgoing longwave radiation (OLR), obtained from the National Oceanic and Atmospheric Administration-Cooperative Institute for Research in Environmental Sciences (NOAA-CIRES) Climate Diagnosis Center [*Liebman and Smith*, 1996].

2.2. WACCM Description

[12] The Whole Atmosphere Community Climate Model, version 4 (WACCM4), is a comprehensive numerical model spanning the range of altitude from the Earth's surface to the thermosphere [*Garcia et al*., 2007]. WACCM4 is based on the framework of the NCAR Community Atmosphere Model, version 4 (CAM4), and includes all of the physical parameterizations of CAM4 [R. B. Neale et al., The mean climate of the community atmosphere model (CAM4) in forced SST and fully coupled experiments, submitted to J. Climate, 2012.] plus a finite volume dynamical core [*Lin*, 2004] for the tracer advection. Recently, a new version of WACCM4 has been constructed to run with specified dynamics (SD) fields [*Lamarque et al*., 2012]. This version of WACCM is ideal for use in comparing species distributions to satellite and aircraft missions. Meteorological fields used in this study are taken from the NASA Global Modeling and Assimilation Office (GMAO) Modern-Era Retrospective Analysis for Research and Applications (MERRA) [*Rienecker et al*., 2011] for January 2004 to December 2010. Here, temperature, zonal and meridional winds, and surface pressure are used to drive the physical parameterizations that control boundary layer exchanges, advective and convective transport, and the hydrological cycle. In this study, the WACCM4 meteorological fields are "nudged" with the SD meteorological fields using the approach described in *Kunz et al*. [2011]. The model has a horizontal resolution of 1.9° latitude × 2.5° longitude and has 88 levels up to about 150 km.

[13] The chemical module of WACCM4 is based upon the 3-D chemical transport Model of Ozone and Related Chemical Tracers, Version 3 (MOZART-3) [*Kinnison et al*., 2007]. WACCM4 includes a detailed representation of the chemical and physical processes in the troposphere through the lower thermosphere. The species included within this mechanism are contained within the Ox, NOx, HOx, ClOx, and BrOx chemical families, along with CH_4 and its degradation products. In addition, fourteen primary nonmethane hydrocarbons and related oxygenated organic compounds are included [*Emmons et al*., 2010]. This mechanism contains 122 species, more than 220 gas-phase reactions, 71 photolytic processes, and 18 heterogeneous reactions on multiple aerosol types. Reaction rates have been updated to JPL-2006 [*Sander et al*., 2006]. Surface emissions are specific to each year, with monthly average biomass burning emissions from the GFED-v2 inventory

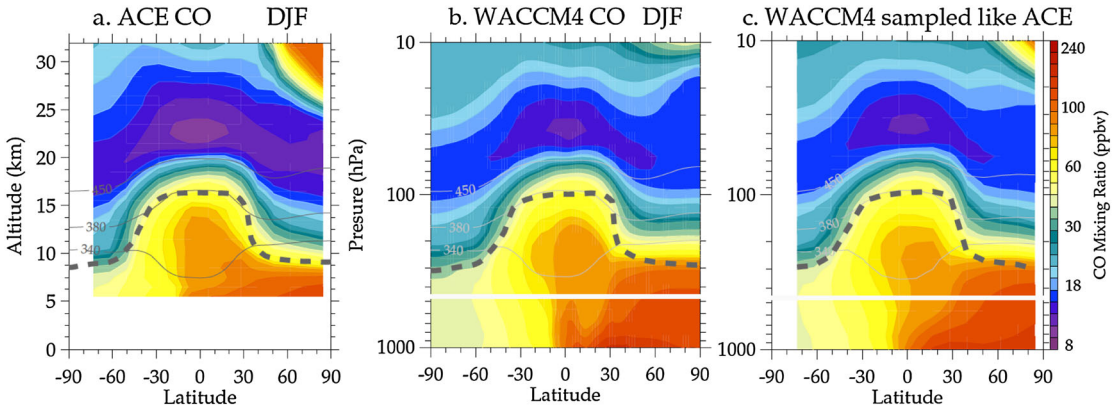

Figure 1. Zonal mean cross sections of carbon monoxide (CO) mixing ratio (ppbv) obtained from (a) ACE-FTS, (b) WACCM4, and (c) WACCM4 sampled like ACE-FTS averaged for December, January, and February (DJF). Thick dashed lines denote the tropopause and thin solid lines denote isentropes (340, 380, and 450 K). Thick solid line in Figure 1b denotes approximate altitude of the lowest level of the ACE-FTS CO in Figure 1a.

[*van der Werf et al*., 2010]. Fossil fuel and biofuel combustion emissions are constant year-round. The emissions are the same as those described in *Emmons et al*. [2010] and *Lamarque et al*. [2012]. Anthropogenic emissions are based on the POET (Precursors of Ozone and their Effects in the Troposphere) database for 2000 [*Granier et al*., 2005], with emissions in Asia replaced by the Regional Emission inventory for Asia (REAS) with the corresponding annual inventory for each year simulated [*Ohara et al*., 2007]. Biogenic emissions of isoprene and monoterpenes are based on MEGAN [*Guenther et al*., 2006, 2012]. While the POET and REAS inventories may be a bit out of date, global annual totals are similar to more recently compiled inventories, such as the ACCMIP historical inventory [*Lamarque et al*., 2010]. In particular, little progress has been made in improving and updating volatile organic compound (VOC) speciated emissions.

[14] HCN emissions were estimated by scaling CO emissions from biomass burning and biofuel combustion using HCN/CO = 0.006 mol/mol [*Akagi et al*., 2011]. HCN has chemical loss with both $O(^1D)$ and OH along with wet deposition in the troposphere and dry deposition over the ocean.

3. Results

3.1. Carbon Monoxide

[15] The behavior of carbon monoxide serves as a backdrop for analyzing other tropospheric hydrocarbons (which often have similar sources as CO), and additionally allows comparisons between CO measurements from ACE-FTS and MLS to quantify the sampling uncertainties of the ACE-FTS data. A zonal mean cross section of CO obtained from ACE-FTS is shown in Figure 1a and compared with WACCM4 (Figure 1b) for Northern Hemisphere (NH) winter (DJF). Overall behavior shows maximum CO mixing ratio in the NH troposphere, due to natural and anthropogenic sources over the continents and relatively slow photochemical loss in wintertime [see *González Abad et al*., 2011]. There are also relatively high values in the tropics related to surface emissions coupled to deep convection, which transport CO rich air from the surface into the upper troposphere [e.g., *Pickering et al*., 1996; *Jiang et al*., 2007]. CO decreases with altitude in the tropical lower stratosphere due to reactions with OH, reaching a minimum near 22 km in the ACE-FTS data, and increases at higher altitudes as a result of methane oxidation. Zonal average CO from WACCM4 simulations (Figure 1b) shows good agreement with ACE-FTS in almost all details. Elevated CO in the Arctic middle stratosphere is seen in the ACE-FTS (above 25 km), which is caused by downwelling of CO rich air from the mesosphere during NH winter. WACCM4 CO also shows a similar pattern near 10 hPa in the Arctic but with significantly smaller magnitude, and much of these differences are tied to the ACE-FTS sampling (with Arctic observations primarily in late January to February). The zonal average CO from WACCM4 sampled like ACE-FTS (Figure 1c) shows similar behavior to the full seasonal zonal means (Figure 1b), but there are higher CO values in the Arctic middle stratosphere, in better agreement with ACE-FTS. The CO-rich air from the polar mesosphere is descended down to 25 km altitude during NH winter [*Funke et al*., 2009]. Zonal mean mixing ratios of CO from both ACE-FTS and WACCM4 in all the other seasons have very similar overall structure to the DJF patterns in Figure 1, with maxima in the NH troposphere and minima in the tropical lower stratosphere. In the Southern Hemisphere (SH) subtropical troposphere there is an additional maximum in Austral spring due to biomass burning emissions over South America and South Africa in both ACE-FTS and WACCM4 (figures not shown).

[16] Seasonal variations of CO in the tropics are mainly influenced by changes in local emissions, convection, large-scale atmospheric circulation, and maximum values are observed in the upper troposphere during equinox seasons [*Duncan et al*., 2003, 2007; *Liu et al*., 2007; *Liu et al*., 2010]. Climatological variations of zonal average CO mixing ratios in the tropical upper troposphere are shown in Figure 2, comparing results from ACE-FTS (at 13.5 km, for the available observations for each month), MLS, and WACCM4 (147 hPa, for all months). The results in Figure 2 are separated for latitude bands 15–30°N, 15°N–15°S, and 30–15°S to highlight respective seasonal variations in different regions. The differences relative to

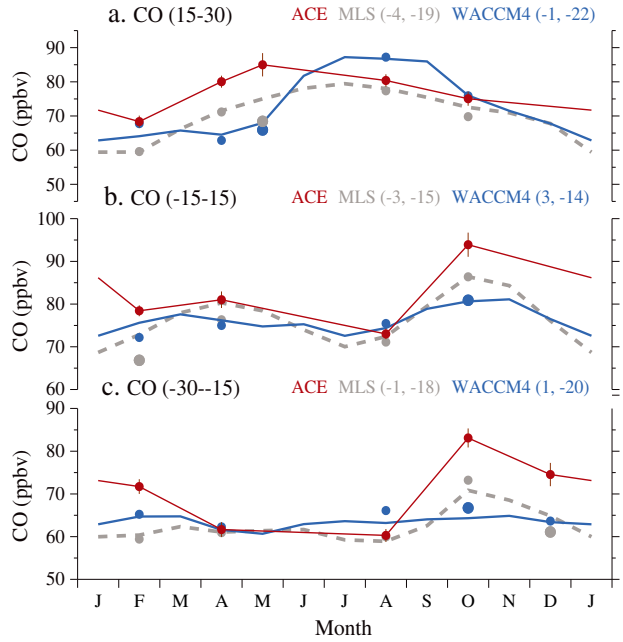

Figure 2. Time series of zonal mean CO mixing ratio climatology (ppbv) obtained from ACE-FTS (red), MLS (gray), and WACCM4 (blue) averaged over (a) 15–30°N, (b) 15°S–15°N, and (c) 30–15°S latitude at 147 hPa (13.5 km for ACE-FTS). Gray and blue solid dots represent average CO from MLS and WACCM4 sampled like ACE-FTS, respectively. The minimum and maximum relative differences between MLS and ACE-FTS (gray) and WACCM4 and ACE-FTS (blue) are shown at each latitude region in percents. The months with maximum difference at each latitude region are marked as slightly larger dots.

ACE-FTS is defined as $\delta X = \frac{X_{ace}-X}{X_{ace}} * 100(\%)$, where δX is mean difference, X is mixing ratio of MLS and WACCM4, and X_{ace} is mixing ratio of ACE-FTS. The CO average in the deep tropics (15°N–15°S) exhibits a semiannual variation with higher mixing ratios in the NH fall (September to November). The SH subtropics (30–15°S) show a maximum during Austral spring associated with enhanced biomass burning emissions [*Duncan et al.*, 2003]. The average CO in the NH subtropics (15–30°N) exhibits a maximum during spring-summer, with summer variations dominated by the region of the Asian monsoon anticyclone [*Randel and Park*, 2006; *Park et al.*, 2009]. The overall patterns show approximate agreement in seasonal variations between the two data sets and WACCM4 with relative differences less than 20%. ACE-FTS CO is, in general, the highest in almost all the latitude regions except NH summer. The differences between ACE-FTS and MLS (and WACCM4) averages in Figure 2 tend to be greater in spring seasons. ACE-FTS CO mixing ratio is up to 19% higher than MLS in April and May in Figure 2a and WACCM4 is underestimated up to 22%, compared to ACE-FTS in October. WACCM4 underestimates the CO maxima in both hemispheric spring seasons, possibly due to underestimation of surface CO emissions, as suggested in previous modeling studies [*Shindell et al.*, 2006; *Duncan et al.*, 2007; *Kopacz et al.*, 2010; *Liu et al.*, 2010]. These studies also suggest that underestimates in the model can be related to the relatively weaker convective transport and/or stronger sink due to OH in the model. Also included in the figure are the MLS and WACCM4 CO sampled like ACE-FTS, then averaged for the available months (shown as gray and blue solid dots in the figure, respectively) to address possible biases due to ACE-FTS sampling. Applying ACE-FTS sampling to MLS and WACCM4 does not change the zonal mean values in Figure 2 significantly. Months with fewer ACE-FTS samples in the tropics show relatively larger differences (e.g., May in Figure 2a and February in Figure 2b). These comparisons demonstrate that ACE-FTS is able to represent seasonal variations in the tropical upper troposphere in spite of its limited sampling.

[17] The horizontal structure of the equinox season's (MAM and SON) average CO mixing ratios in the upper troposphere, obtained from ACE-FTS and MLS data, are shown in Figures 3 and 4, together with the WACCM4 results. Shown on the left panel of Figure 3 are the seasonal average CO based on the gridded data sets for MAM. In the right panel of Figure 3 we show ACE-FTS measurement locations for MAM (Figure 3b) and seasonal average CO from MLS and WACCM4 with ACE-FTS sampling applied (Figures 3d and 3f). Figures 3a, 3c, and 3e also highlight the location of climatological deep convection (low OLR, shown as white contours), showing maxima of convective activity over the continents (North Africa, Indonesia, and South America). The comparisons between ACE-FTS and MLS data (Figures 3a and 3c) show reasonable agreement in terms of patterns and magnitudes, although there are some differences in detail likely attributable to the limited sampling of ACE-FTS and differences in vertical resolution. The maxima in upper tropospheric CO are located in the regions nearby the convective maxima; CO surface emissions (mostly biomass burning) are also colocated with the seasonally varying tropical deep convection [*Duncan et al.*, 2003], which contributes to the correlated behavior in the different data sets. The seasonal averages for the WACCM4 simulation (Figure 3e) demonstrate similar spatial structures as those seen in ACE-FTS and MLS data.

[18] The measurement locations for ACE-FTS (shown as solid squares in Figure 3b) show relatively sparse sampling in lower latitudes and over convective regions, but there is coverage over all longitudes for these multiyear averages. We applied ACE-FTS sampling to the MLS and WACCM4 CO to account for the bias from limited sampling of ACE-FTS. This does not change spatial distributions of CO significantly (Figures 3d and 3f), except for a slight decrease in CO maxima in the tropics. Quantitative comparisons show ACE-FTS CO is higher than both MLS and WACCM4 (by approximately 10%–15%) in the tropics and lower in the higher latitudes (especially for MLS; the large differences in high latitude are probably related to the broader vertical weighting for MLS observations).

[19] Overall there is reasonable agreement between the ACE-FTS climatology and MLS results in Figure 3, suggesting that the ACE-FTS data are adequate to quantify the large-scale horizontal structure for seasonal averages. In Figure 4, seasonal averages of CO from ACE-FTS, MLS, and WACCM4 are shown for Austral spring (September to November), and these comparisons show similar behavior to the MAM results (Figure 3). Some specific differences

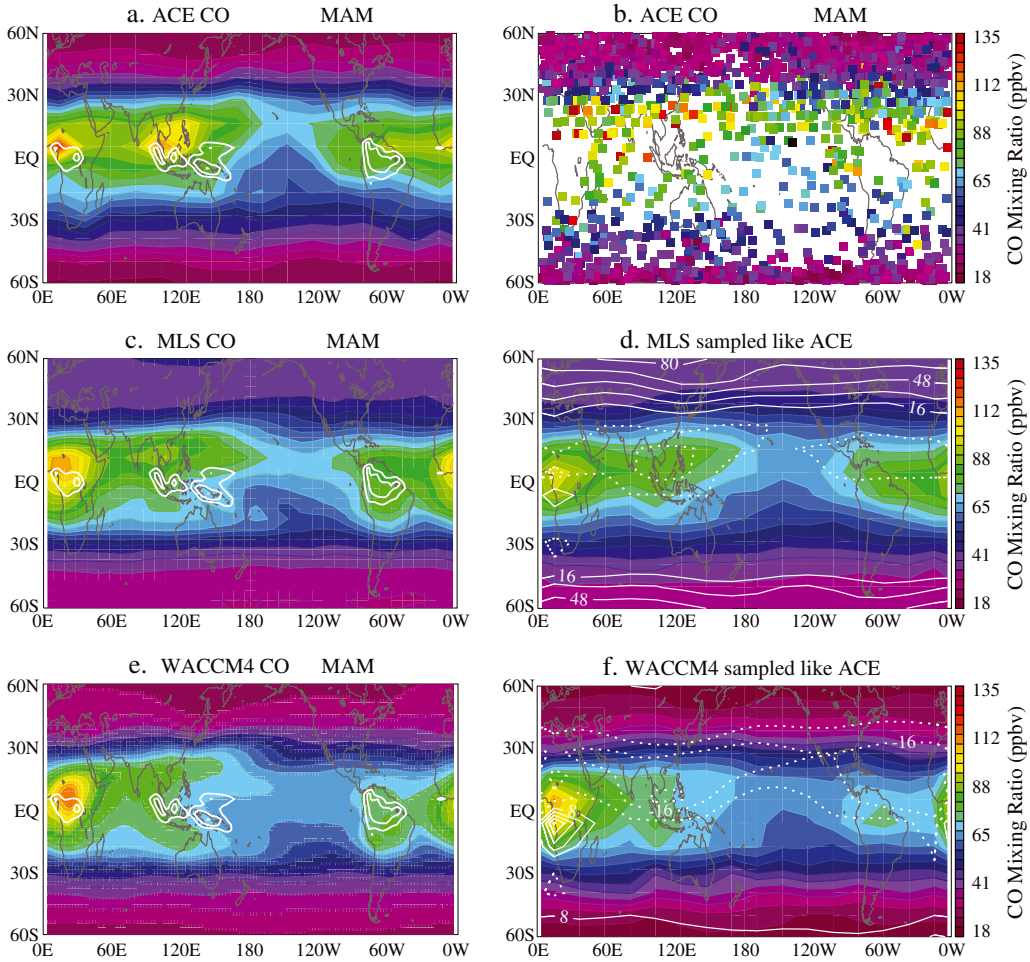

Figure 3. Horizontal structures of CO mixing ratio (ppbv) obtained from (a) ACE-FTS at 13.5 km, (c) MLS, and (e) WACCM4 at 147 hPa averaged for March, April, and May (MAM). White contours indicate seasonal average of OLR ($\leq$220 Wm^{-2}), indicative of climatological deep convection. (b) ACE-FTS measurement locations at 13.5 km during MAM colored by CO mixing ratios. Figures 3d and 3f are MLS and WACCM4 CO sampled like ACE-FTS then gridded at 147 hPa, respectively. White contours indicate relative differences between (d) MLS and ACE-FTS and (f) WACCM4 and ACE-FTS shown as percents (negative values are shown as dotted lines). Contour intervals for positive values in Figure 3d are twice as big as the one in Figure 3f.

for SON include lower CO maxima in the SH subtropics (especially near South America) for both MLS and WACCM4 (up to 20%) compared to ACE-FTS. The difference with MLS near South America suggests lower vertical resolution of the MLS data, but it is within the range of systematic uncertainty of the MLS CO data [*Livesey et al.*, 2011]. Low model values suggest an underestimate of surface CO emission and/or insufficient vertical transport over this region. On the other hand, WACCM4 overestimates CO over the Asian monsoon region (positive differences over Asia in Figure 4f); this occurs because the summertime (JJA) maximum persists into SON in the model (more so than in the satellite observations).

[20] Further details of the climatological seasonal behavior of CO in the tropical (15°N–15°S) upper troposphere, based on the monthly MLS climatology, are shown in Figure 5a; these data highlight the semiannual maxima (MAM and SON) that occur primarily over continental regions (Africa, Indonesia, and South America). MLS CO shows maxima over all three continents in Austral spring and a more pronounced maximum over Africa in Boreal spring. A similar diagnostic for WACCM4 (Figure 5b) shows patterns consistent with these observations; the model patterns match MLS for the maximum over Africa during MAM, but weaker model maxima are found during SON (especially over South America). The differences between Figures 5a and 5b are typically $\pm$10%, and up to 20% over South America during SON.

[21] One prominent seasonal feature of CO in the UTLS is the strong maximum during NH summer (JJA) associated with the Asian summer monsoon anticyclone, as documented in *Li et al.* [2005] and *Park et al.* [2007, 2008]. This feature is linked to transport of surface pollution in monsoonal deep convection and confinement within the strong anticyclonic circulation in the UTLS. *Park et al.* [2009] furthermore show that a CTM can simulate the large-scale behavior of CO in this region reasonably well. Comparisons of WACCM4 with MLS and ACE-FTS (Figures 2–5)

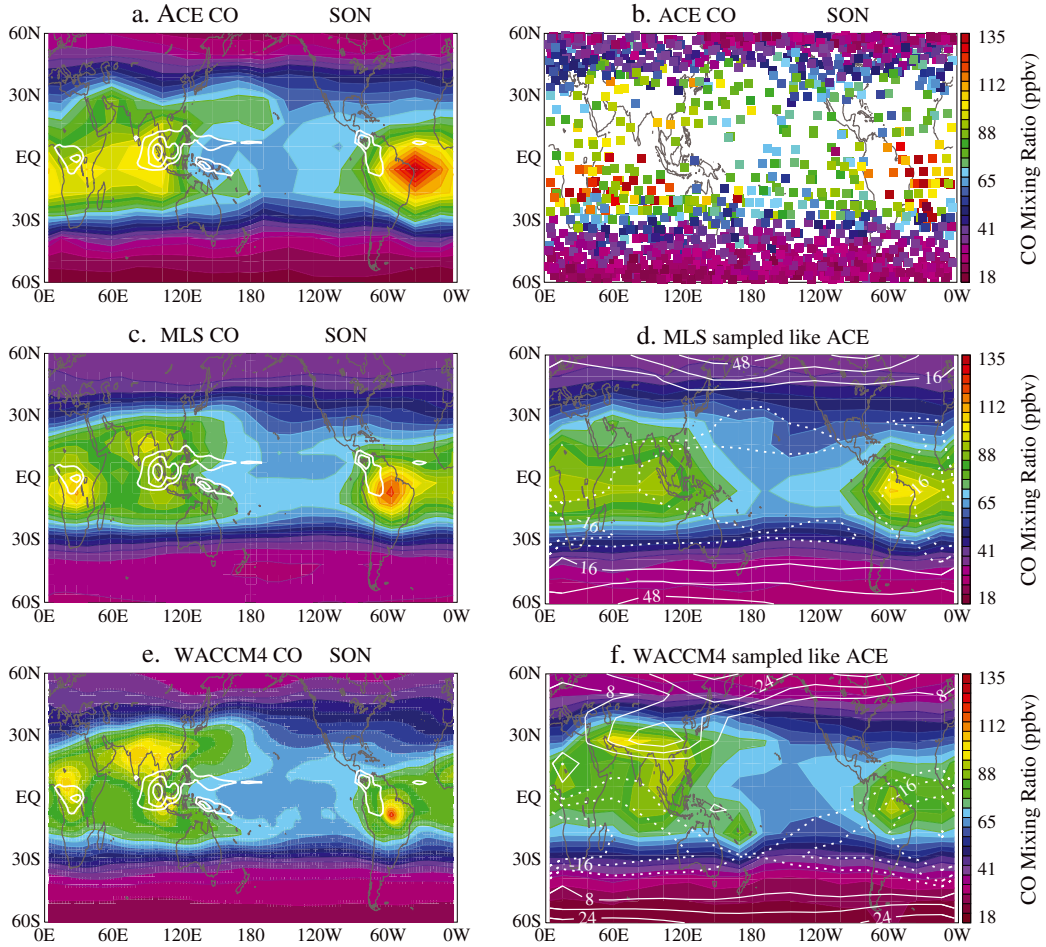

Figure 4. Same as Figure 3 but for seasonal averages for September, October, and November (SON).

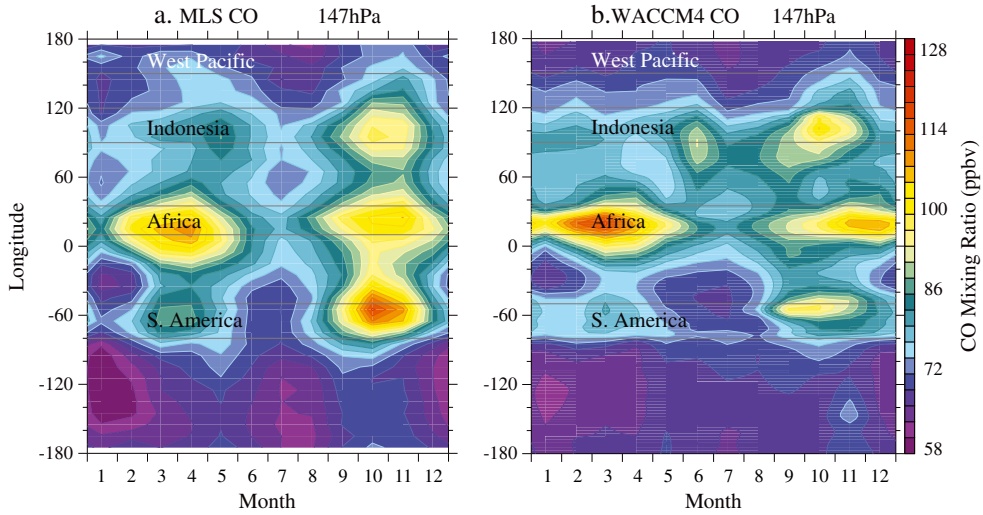

Figure 5. Time and longitude variations of tropical average (15°S–15°N) CO mixing ratios (ppbv) obtained from (a) MLS and (b) WACCM4 at 147 hPa, respectively. Thin gray lines denote geographical locations of tropical deep convective regions (West Pacific, Indonesia, Africa, and South America).

indicate that the model reproduces seasonal cycle of CO reasonably well, but overestimates CO over Southeast Asia during NH summer (Figure 5). This is different from both Boreal and Austral spring season comparisons, where WACCM4 slightly underestimates CO mixing ratios in the upper troposphere.

[22] Seasonal and interannual variability of zonal mean tropical (15°N–15°S) CO from the longer record of ACE-FTS, MLS, and WACCM4 data (2004–2010) are shown in Figure 6 for individual pressure levels spanning 68–215 hPa. The seasonal cycle of tropical CO consists of an annual cycle of lower level mixing ratios (maximum during NH fall–winter, due to enhanced NH emissions and slow photochemistry) [see Duncan *et al*., 2007] transitioning to a semiannual variation in the upper troposphere, related to transport through continental deep convection (Figure 5). This semiannual cycle is most evident in the MLS data at 147 and 100 hPa in Figure 6. Note the enhanced CO values during late 2006 are related to stronger biomass burning emissions during the corresponding ENSO event [*Logan et al*., 2008; *van der Werf et al*., 2010; *Liu et al*., 2010; *Zhang et al*., 2011]. There is very good agreement between the ACE-FTS and MLS data and the WACCM4 simulation for pressure levels 215 and 147 hPa in Figure 6 (relative differences are less than 7%). Somewhat larger differences occur in these comparisons at the 100hPa level, with larger mean biases between ACE-FTS and MLS (MLS being 23% higher than ACE-FTS), and larger amplitude in seasonal variations in MLS compared to both ACE-FTS and WACCM4. In the lower stratosphere (68 hPa), the dominant variability in CO is an annual cycle with maximum in the NH winter, linked to the seasonal maximum in upwelling across the tropical tropopause [*Randel et al*., 2007]. The annual cycle in the tropical upwelling in WACCM4 is in good agreement with observations [as shown by *Taguchi*, 2009] consistent with the accurate simulation of CO variability at 68 hPa (difference is less than 1%). MLS CO is higher than both ACE-FTS (up to 17%, which is within the range of systematic uncertainty of the MLS CO) [see *Clerbaux et al*., 2008] and WACCM4 at this pressure level.

[23] The comparisons in Figures 2–6 demonstrate that ACE-FTS has the ability to capture much of the seasonal space-time variability in the tropical UTLS (compared with MLS data), in spite of limited sampling in the tropics (i.e., only four times per year). Overall the ACE-FTS and MLS data show good agreement, although ACE-FTS CO mixing ratios in the tropics are systematically lower than MLS at 100 and 68 hPa and slightly lower at 215 hPa. Vertical profiles of tropical average CO from ACE-FTS and MLS are shown in Figure 7, together with WACCM4 results and a tropical climatology derived from research aircraft measurements [from *Tilmes et al*., 2010]. MLS CO is shown at each of the retrieval pressure levels with solid vertical lines to emphasize the vertical resolution of the data. The differences between MLS and WACCM4 relative to ACE-FTS average CO are shown at each MLS pressure level in percents. Both MLS and WACCM4 agree within 7% in the upper troposphere; MLS is biased high at 68 hPa (~30%) and WACCM4 is biased high (~25%) at 46 hPa compared to ACE-FTS. It is noteworthy that there is reasonable agreement in vertical gradients and magnitudes

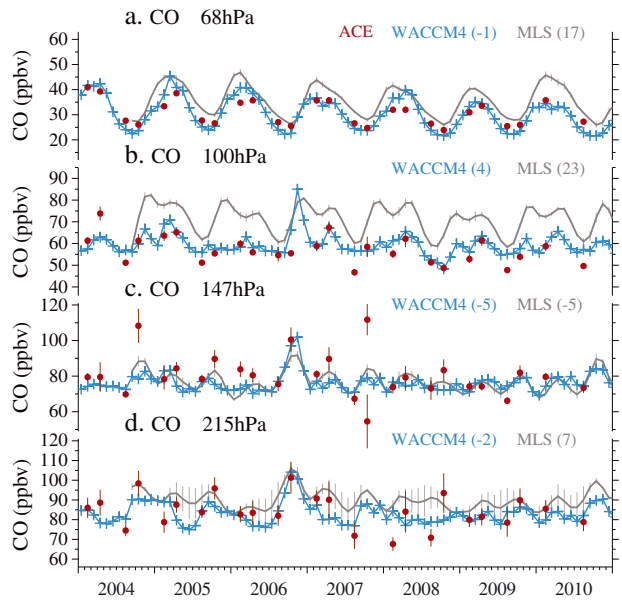

Figure 6. Monthly mean time series of CO mixing ratios (ppbv) at (a) 68, (b) 100, (c) 147, and (d) 215 hPa obtained from MLS (gray), ACE-FTS (red dots), and WACCM4 (light blue) averaged over 15°S–15°N, respectively. Error bars represent one sigma standard deviation of the monthly averages. The average relative differences between WACCM4 and ACE-FTS (blue) and MLS and ACE-FTS (gray) are shown at each pressure level in percents. Note that ACE-FTS measurements in the tropics are only available four times per year (February, April, August, and October) due to the satellite's orbit geometry.

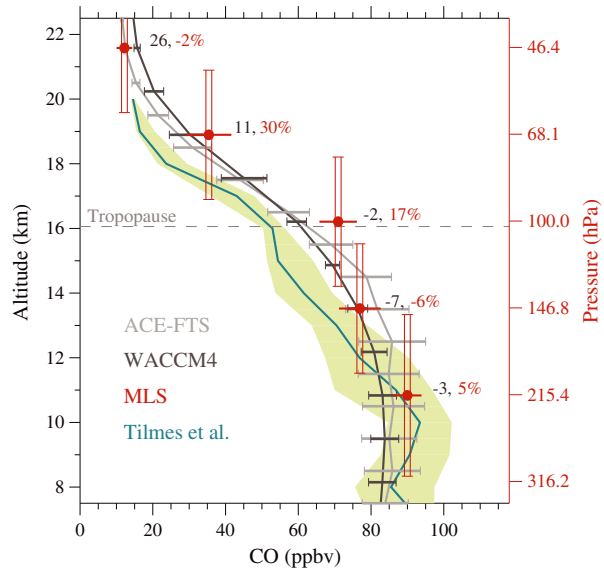

Figure 7. Vertical profiles of annual average CO mixing ratio (ppbv) obtained from ACE-FTS (gray), MLS (red), and WACCM4 (dark gray) averaged in 15°S–15°N. Error bars indicate one sigma standard deviation of the annual averages at each level. Tropical CO climatology from *Tilmes et al*. [2010] is shown as aquamarine solid line and the estimated uncertainties are shown as light green shadings. The relative differences between WACCM4 and ACE-FTS (gray) and MLS and ACE-FTS (red) are shown at each MLS pressure level in percents. Gray dashed lines indicate annual average tropical tropopause height obtained from NCEP/NCAR reanalysis.

of CO from all three measurements (ACE-FTS, MLS, and combined aircraft climatology) and the WACCM4 simulation, in spite of limitations in the sampling of ACE-FTS and vertical resolution of MLS. MLS CO at 100 hPa is higher than ACE-FTS (17%), which is consistent with CO comparisons shown by *Clerbaux et al*. [2008].

3.2. Ethane and Acetylene

[24] Ethane (C_2H_6) is produced as a result of fossil fuel, biofuel, natural gas, and biomass burning [*Rinsland et al*., 1998; *Xiao et al*., 2008] and has a lifetime of ~45 days [*Zhao et al*., 2002]. Due to its relatively long lifetime in the troposphere, C_2H_6 has been used as a tracer for fire emission and transport [*Rinsland et al*., 2005; *Park et al*., 2008]. Acetylene (C_2H_2) has similar sources to C_2H_6, but a substantially shorter lifetime of ~2 weeks in the troposphere [*Xiao et al*., 2007], which makes it an interesting complementary observation for transport. While these tracers share certain features with CO (as shown below), they are different in that they primarily originate from surface emissions, whereas CO also has a photochemical source in the troposphere (accounting for about one-half of the CO burden).

[25] Zonal mean cross sections of C_2H_6 mixing ratio obtained from ACE-FTS and WACCM4 averaged for NH winter (DJF) are shown in Figures 8a and 8b. In general, C_2H_6 has a similar zonal mean structure with CO (see Figure 1), except that it decreases monotonically in the lower stratosphere, as there is no additional source above the tropopause. In the troposphere, C_2H_6 has a maximum in the NH related to enhanced emissions and longer photochemical lifetimes in the reduced radiative environment of winter. WACCM4 C_2H_6 (Figure 8b) shows a similar distribution to the ACE-FTS observation, but with lower mixing ratios both in the troposphere (up to 60% lower in the upper troposphere) and in the lower stratosphere. Calculation of the WACCM4 averages using ACE-FTS sampling (as in Figure 1) gives results that are nearly identical to the full zonal averages (not shown). Figures 9a–9c compare the monthly climatologies of C_2H_6 at 147 hPa from WACCM4 with available ACE-FTS measurements at 13.5 km for tropical latitude bands (as in Figure 2). This comparison reveals a systematic underestimate for WACCM4 throughout all the latitudes. The relative differences between WACCM4 and ACE-FTS range from -16% in the SH subtropics (Figure 9c) to -53% in the NH subtropics (Figure 9a). The underestimation of C_2H_6 in the model is the largest in both hemispheric spring seasons, when the observations show maxima that are absent in WACCM4. (This is similar to the underestimation of CO in WACCM4 for this season as discussed above.) It is possible that surface emission of C_2H_6 is underestimated in

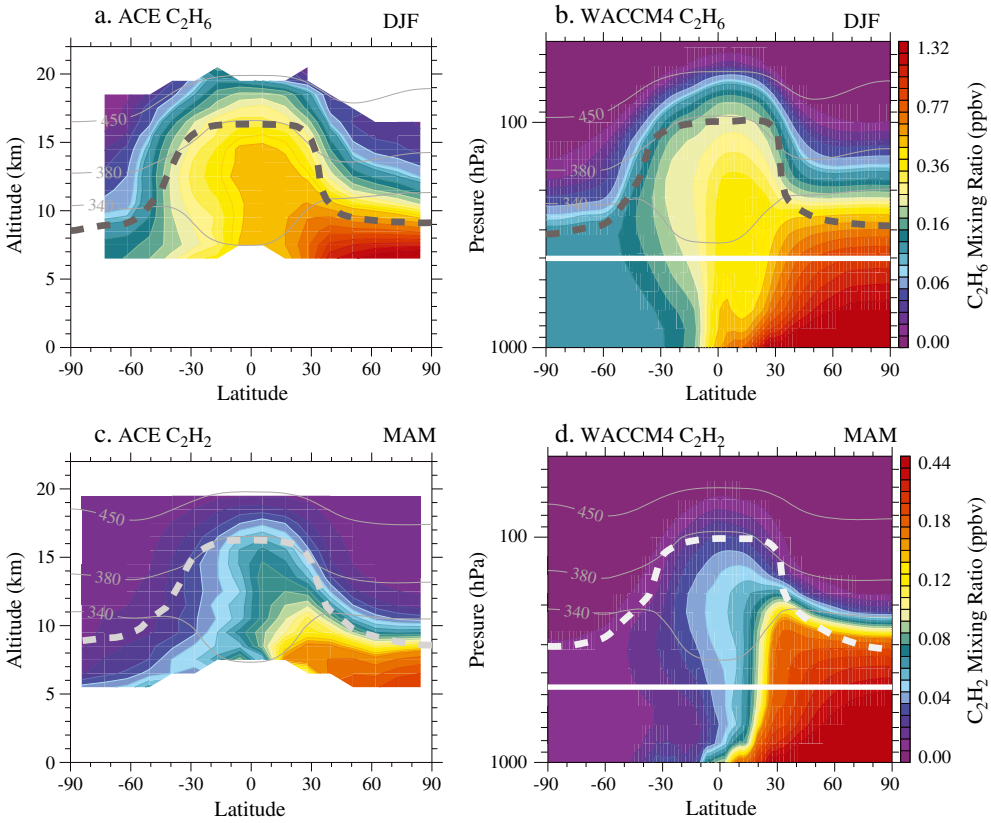

Figure 8. Zonal mean cross sections of (a and b) ethane (C_2H_6) mixing ratios (ppbv) averaged from December to February (DJF) and (c and d) acetylene (C_2H_2) mixing ratios (ppbv) averaged from March to May (MAM) obtained from (a and c) ACE-FTS and (b and d) WACCM4, respectively. Thin solid lines represent isentropes (340, 380, and 450 K). Thick solid lines in Figures 8b and 8d denote approximate altitudes of the lowest level of the ACE-FTS data in Figures 8a and 8c, respectively.

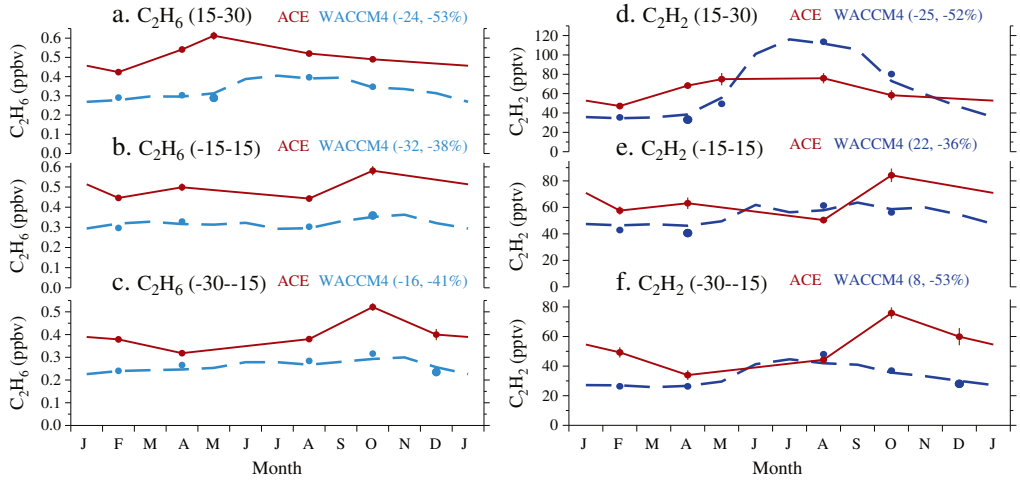

Figure 9. (Left) Time series of zonal mean C_2H_6 mixing ratio (ppbv) climatology obtained from ACE-FTS (red) and WACCM4 (blue) averaged over (a) 15–30°N, (b) 15°S–15°N, and (c) 30–15°S at 147 hPa (13.5 km for ACE-FTS), respectively. (Right) Same as (left) but for C_2H_2 mixing ratio (ppbv). Blue solid dots represent WACCM4 C_2H_6 and C_2H_2 sampled like ACE-FTS, respectively. The maxima and minima of relative differences between WACCM4 and ACE-FTS are shown as percents at each latitude region and the months with the maximum difference are marked as slightly larger dots.

the model due to large uncertainties in current emission inventory [*Duncan et al.*, 2007; *Kopacz et al.*, 2010] and complex chemistry and transport in the global models [*Shindell et al.*, 2006]. Again, applying ACE-FTS samplings to the WACCM4 C_2H_6 simulations does not have a big impact on estimated seasonal variations (shown as blue dots in the figure).

[26] Seasonal averages of C_2H_6 in the upper troposphere exhibit similar regional climatological maxima as CO (e.g., Figures 3–5), linked to regions of deep convection (figures not shown). The correlated behaviors in CO and C_2H_6 are highlighted in scatter plots for the tropical (15°N–15°S) upper tropospheric measurements from ACE-FTS, with measurements separated for the upper troposphere (8.5–14.5 km) and lower stratosphere (15.5–19.5 km) for NH spring (Figure 10a). The overall correlation between CO and C_2H_6 is due to common sources (e.g., biomass burning) and their similar photochemical lifetimes in the troposphere [*Marcy et al.*, 2004; *Turquety et al.*, 2008; *Wiegele et al.*, 2012]. Figure 10b shows a similar correlation plot for WACCM4 results; here we only included WACCM4 daily data sampled at the ACE-FTS measurement locations for this season (March–May). WACCM4 reproduces the observed correlation between C_2H_6 and CO in the tropics (Figure 10a) with somewhat lower correlation slopes (0.0064 vs. 0.0047). The linear least square fit based on the ACE-FTS CO and C_2H_6 data in Figure 10a is shown in both panels for comparison. The fit estimated from WACCM4 (dashed line in Figure 10b) illustrates that WACCM4 underestimates C_2H_6 compared to CO. Both correlation coefficient and standard error (sigma) are comparable from ACE-FTS and WACCM4.

[27] C_2H_2 has similar overall behavior to CO and C_2H_6, but with more pronounced hemispheric differences and more rapid drop-off across the tropopause (Figures 8c and 8d) due to a shorter chemical lifetime. There is overall agreement between the WACCM4 simulation and ACE-FTS behavior in the troposphere, with average relative difference of ~30% in the tropical upper troposphere. WACCM4 underestimates C_2H_2 in most of the troposphere except the NH polar region, where WACCM4 is up to 90% higher than ACE-FTS. In the seasonal averages, the WACCM4 values of C_2H_2 at 147 hPa are generally lower (up to 53%) than ACE-FTS, and the differences are seasonally dependent (Figures 9d–9f). WACCM4 overestimates C_2H_2 in the NH subtropics during summer (in the Asian monsoon anticyclone) and underestimates in the subtropics during both hemispheric springs, which is consistent with the results from CO and C_2H_6 (Figures 2 and 9a–9c). The overestimation in summer and underestimation in spring in NH subtropics (Figure 9d) result in a somewhat different seasonal cycle in C_2H_2 in WACCM4 compared to ACE-FTS. Both C_2H_6 and C_2H_2 are strongly correlated with CO in the tropical upper troposphere and in the lower stratosphere (Figure 10). However, the associated regression line does not approach the origin, as there is a substantial amount of CO in regions where almost no C_2H_6 or C_2H_2 exist (due to the in-situ photochemical sources of CO in the troposphere).

[28] Figures 11a and 11b show zonal mean vertical profiles of annual average C_2H_6 and C_2H_2 obtained from ACE-FTS and WACCM4 averaged in the tropics (15°S–15°N), respectively. The range of seasonal averages (i.e., minimum and maximum) is denoted as a horizontal line at each altitude (pressure for WACCM4). Absolute values of C_2H_6 and C_2H_2 are higher in the ACE-FTS measurements than WACCM4, as noted above (~28 % for both C_2H_6 and C_2H_2 at the tropopause). Mixing ratios of C_2H_6 and C_2H_2 decrease rapidly with altitude in the upper troposphere (above ~14 km), and there is qualitative agreement in the vertical gradients of C_2H_6 and C_2H_2 from both the measurements and the model.

[29] Chemical reaction with atomic chlorine (Cl) is an important sink of the C_2H_6 in the lower stratosphere due to temperature dependency of the reaction [*Aikin et al.*, 1982]. The effects of chlorine chemistry are illustrated by comparing the vertical profile of C_2H_6 from a previous version of WACCM4 that excluded the effects of chlorine

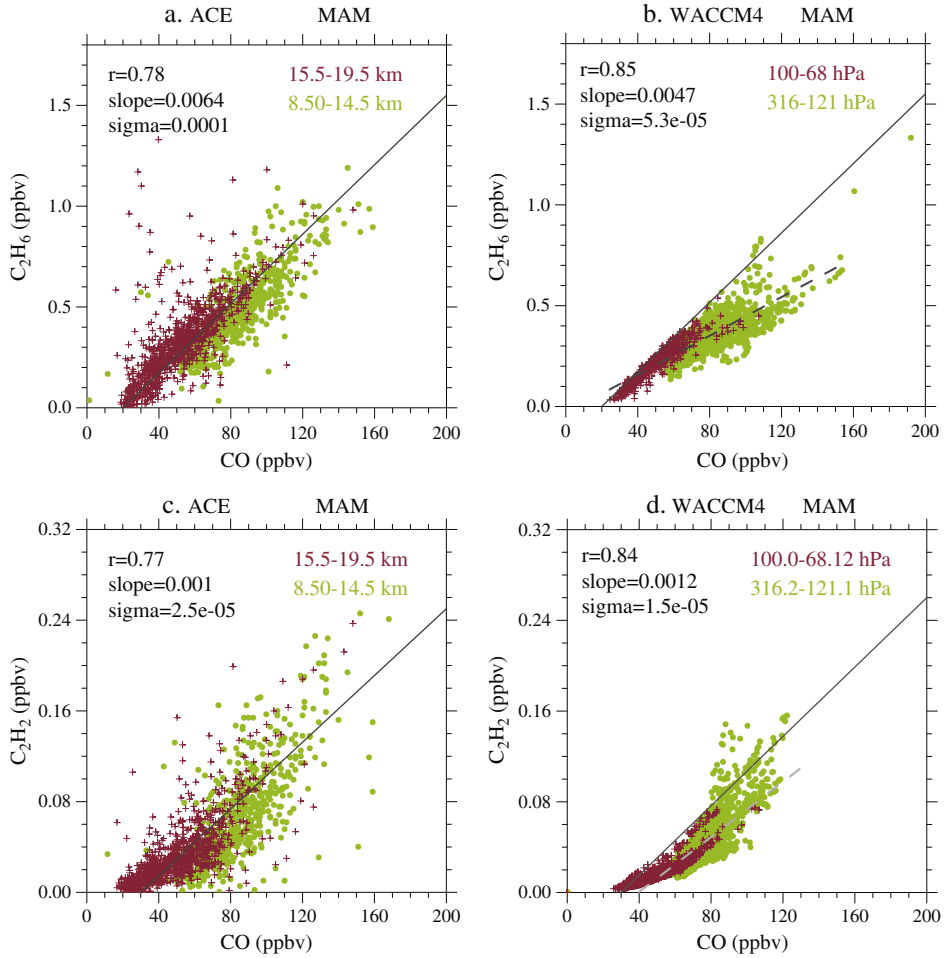

Figure 10. Scatter plots of (top) CO vs. C_2H_6 and (bottom) CO vs. C_2H_2 in the tropics (15°S–15°N) obtained from (left) ACE-FTS and (right) WACCM4 sampled as ACE-FTS (see text for detail) for March–May (MAM). Red crosses represent stratospheric (15.5–19.5 km for ACE-FTS and 100–68 hPa for WACCM4) and the solid green dots represent upper tropospheric (8.5–14.5 km for ACE-FTS and 316–121 hPa for WACCM4) air masses, respectively. Linear least square fits estimated from the ACE-FTS measurements are shown as solid gray lines; these same lines are shown in the WACCM4 panels. Gray dashed lines represent linear regression fit using WACCM4. Correlation coefficient, slope, and one sigma standard deviation are shown in the upper left corners.

chemistry, specifically the reaction of $C_2H_6 + Cl$, with the current simulation. The rate constant information for this reaction was taken from *Sander et al.* [2006]. Figure 11a includes the vertical profile of C_2H_6 from that simulation (shown as gray dots), showing slightly higher values in the troposphere but a very different vertical structure in the lower stratosphere, with slower decrease with height compared to the current WACCM4 simulation and ACE-FTS measurements. With the current simulation, C_2H_6 mixing ratio becomes almost zero at ~22 km, but without the chlorine chemistry C_2H_6 mixing ratios remain high well into the stratosphere. We conclude that the effects of chlorine chemistry are important for quantitatively understanding the behavior of C_2H_6 in the lower stratosphere.

[30] Long-term variations of C_2H_6 and C_2H_2 in the tropical (15°S–15°N) lower stratosphere (at 68 hPa) are shown in Figures 12b and 12c, comparing the available ACE-FTS data (four monthly samples per year) with monthly WACCM4 results over 2004–2010. Note that the available ACE-FTS data in each month is dependent on species and altitude (4–21 per month for C_2H_6 and 7–51 for C_2H_2). Due to fewer numbers of available samples, C_2H_6 has greater scatter and variability than C_2H_2 from ACE-FTS. There is a repeatable annual cycle in both C_2H_6 and C_2H_2 with maxima in the NH spring, which is consistent with the seasonal cycle in CO at this altitude (Figure 6); these annual cycles are a response to variations in the tropical upwelling (Brewer-Dobson circulation). WACCM4 has a reasonable representation of the annual cycles in both tracers with relatively lower mixing ratios (average biases are -61% for C_2H_6 and -64% for C_2H_2, respectively). More work is needed to investigate the impacts of the modeling of these processes on the modeled composition fields.

3.3. Hydrogen Cyanide

[31] The space-time behavior of hydrogen cyanide (HCN) is somewhat distinct from CO, C_2H_6, and C_2H_2 in the tropical UTLS. Although it has similar sources (biomass and

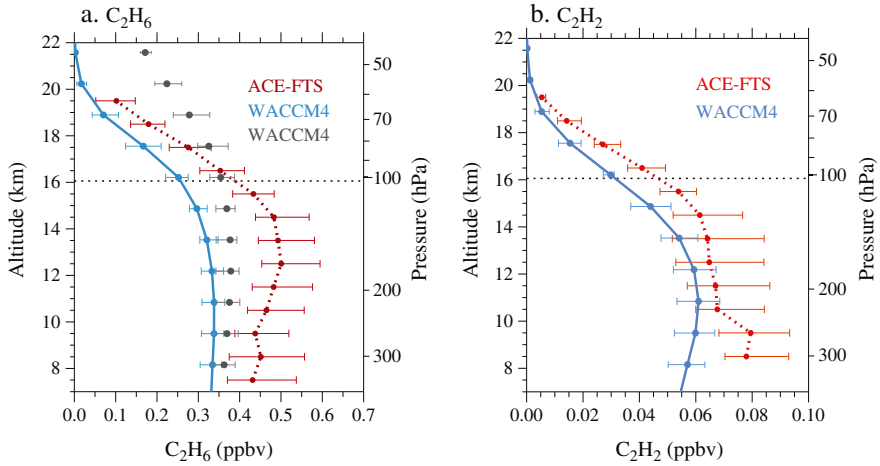

Figure 11. Zonal mean vertical profiles of annual average (a) C_2H_6 (ppbv) and (b) C_2H_2 (ppbv) mixing ratios averaged over 15°S–15°N, for ACE-FTS (red) and WACCM4 simulations (blue). Gray dots in Figure 11a represent WACCM4 simulation of C_2H_6 without chlorine reaction with C_2H_6 included (see text for detail). The range of seasonal averages (minimum and maximum) is marked as thin solid lines at each level. Thin dotted lines denote the annual mean tropical tropopause obtained from NCEP/NCAR reanalysis.

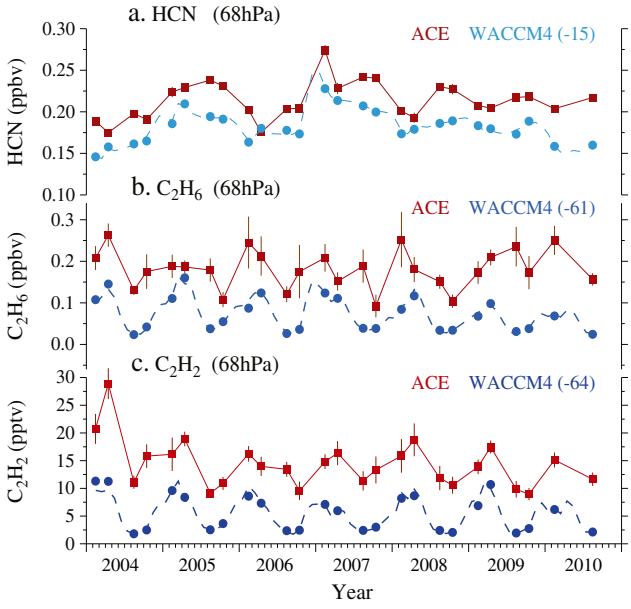

Figure 12. Time series of monthly mean mixing ratios (ppbv) of (a) HCN, (b) C_2H_6, and (c) C_2H_2 obtained from ACE-FTS (at 19.5 km, red) and WACCM4 (68 hPa, blue) averaged over 15°S–15°N, respectively. Solid blue dots represent WACCM4 simulation for each species sampled like ACE-FTS, and the numbers in parentheses represent averages of relative differences between WACCM4 and ACE-FTS in percents. Error bars show one sigma standard deviation of the monthly averages.

biofuel burning) and sinks (reaction with OH and photolysis) in the atmosphere, HCN has a much longer lifetime in the free atmosphere (~4 years). However, HCN also has a significant sink associated with contact with the ocean surface, so that the average tropospheric lifetime of HCN is ~5 months [*Li et al.*, 2003; *Kleinböhl et al.*, 2006]. Horizontal structures of seasonal average ACE-FTS HCN in the upper troposphere show a minimum over the tropical Western Pacific Ocean, which reflects the oceanic sink and rapid transport in tropical convection [see *Randel et al.*, 2010].

[32] Zonal mean structures of seasonal average HCN obtained from ACE-FTS are shown in Figures 13a and 13c, averaged for NH summer (JJA) and SH spring (SON), respectively. HCN mixing ratios higher than 0.4 ppbv are considered to be affected by biomass burning plumes [*Glatthor et al.*, 2009; *Wiegele et al.*, 2012], which is clearly shown in Figures 13a and 13c. Enhanced HCN mixing ratios in the UTLS are observed in the NH extratropics during summer (Figures 13a and 13b), which demonstrates transport pathways from the troposphere into the lower stratosphere associated with the Asian monsoon anticyclone. Both satellite measurements and model simulations have shown that CO mixing ratio is enhanced over Southeast Asia due to the Asian monsoon anticyclone [*Barret et al.*, 2008; *Turquety et al.*, 2008; *Funke et al.*, 2009; *Wiegele et al.*, 2012]. With the relatively long photochemical lifetime in the stratosphere, remnants of this enhanced HCN in the NH last until the next season (Figure 13c). In comparison to shorter-lived species such as CO or C_2H_2, HCN shows a more gradual decrease with altitude above the tropopause. A strong enhancement in HCN is also observed in the SH subtropics during Austral spring (Figure 13c), but the high values do not extend above the tropopause. Overall, WACCM4 HCN shows qualitative agreement with ACE-FTS with maxima in the NH summer and SH spring (Figures 13b and 13d), although the WACCM4 maximum in SH during Austral spring (Figure 13d) is substantially smaller compared to ACE-FTS (consistent with other species shown above).

[33] Temporal variability of HCN in the tropics is highlighted by time-altitude section of zonal mean HCN derived from ACE-FTS (Figure 14a). Note again that ACE-FTS tropical sampling is limited to four months per year, with substantial variability in the number and location of available

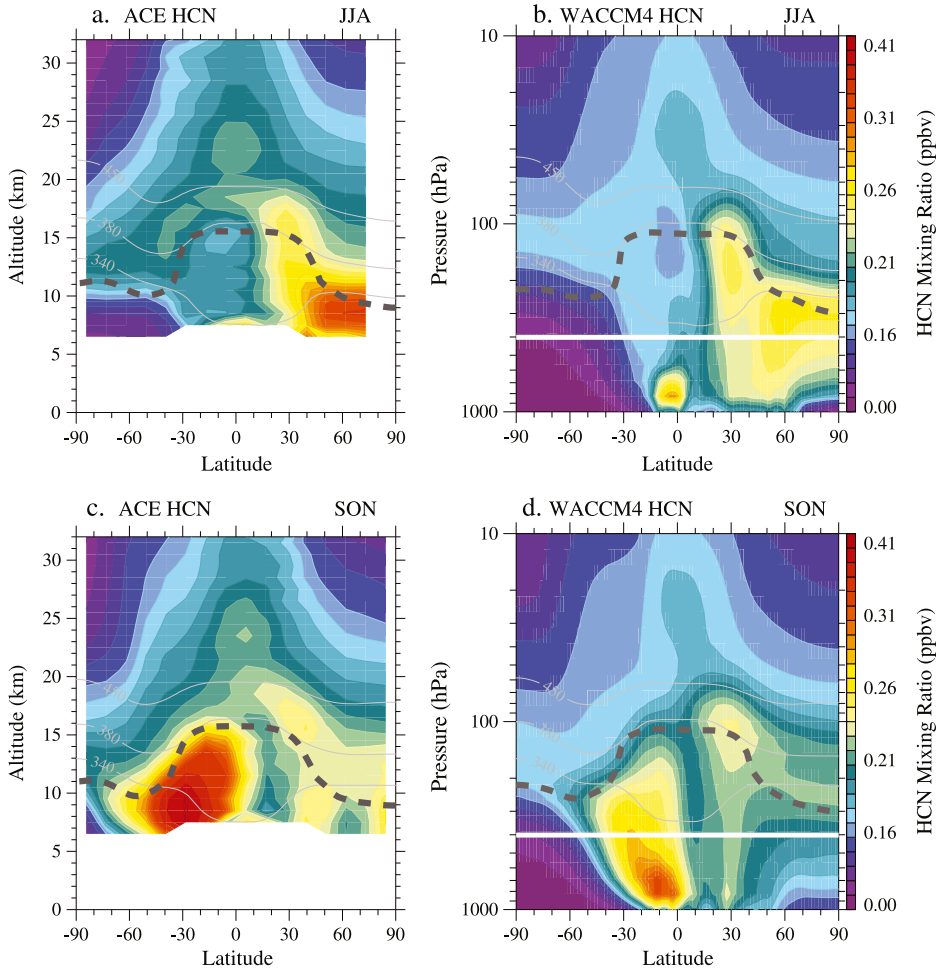

Figure 13. (left) Zonal mean cross sections of HCN mixing ratios (ppbv) obtained from ACE-FTS averaged for (a) June-August (JJA) and (c) September-November (SON), respectively. (right) Same as Figures 13a and 13c but for WACCM4. Thin solid lines denote isentropes (340, 380, and 450 K) and thick dashed lines denote the tropopause. Thick solid lines in Figures 13b and 13d denote approximate altitudes of the lowest level of the ACE-FTS HCN shown in Figures 13a and 13c, respectively.

measurements per month (11–81 per month depending on altitudes for HCN). Variability of HCN in the tropical UTLS is largely influenced by biomass burning events, with seasonal maxima in the NH and SH spring seasons. The largest interannual variability during this time period is related to the enhanced biomass burning event over Indonesia tied to ENSO in 2006 [*Logan et al*, 2008; *van der Werf et al*., 2010; *Zhang et al*., 2011]. The ACE-FTS observations (Figure 14a) show the semiannual cycle in the troposphere but distinct longer-term variations in the stratosphere. Much of the variability in the lower stratosphere originates near the tropical tropopause during NH summer and autumn (denoted with Xs in Figure 14a), linked to transport in the Asian monsoon anticyclone; these stratospheric maxima propagate upwards with the Brewer-Dobson circulation. This behavior is distinct from the seasonal maxima during NH winter/spring observed in CO, C_2H_6, and C_2H_2 (e.g., Figures 6 and 12), which is mainly due to upward transport in the deep tropics. In addition, HCN mixing ratios in the stratosphere show substantial interannual variations, with maxima in 2005 and 2007.

[34] The WACCM4 simulation of HCN shows qualitative agreement with ACE-FTS both in the troposphere and in the lower stratosphere (Figure 14b). In the troposphere, HCN has a semiannual cycle with maxima in each hemispheric spring, with smaller magnitudes compared to ACE-FTS (especially during SON, as discussed above). WACCM4 HCN mixing ratios in the stratosphere are generally lower than ACE-FTS, but the maxima and minima occur at approximately the same time. One additional source for stratospheric HCN could be the conversion of methyl cyanide (CH_3CN) [*Schneider et al*., 1997], which is not included in the current WACCM4 simulation. We note that the HCN maxima in the lower stratosphere during NH summer (marked as crosses) are well reproduced in the model, and again represent transport through the Asian monsoon circulation into the stratosphere (Figure 13).

[35] This distinct behavior of HCN across the tropical tropopause compared to the shorter-lived hydrocarbons is further illustrated in the ACE-FTS HCN vs. CO scatter plots in Figure 15a. In the troposphere, there is a positive correlation ($r = 0.80$) between HCN and CO as they have long

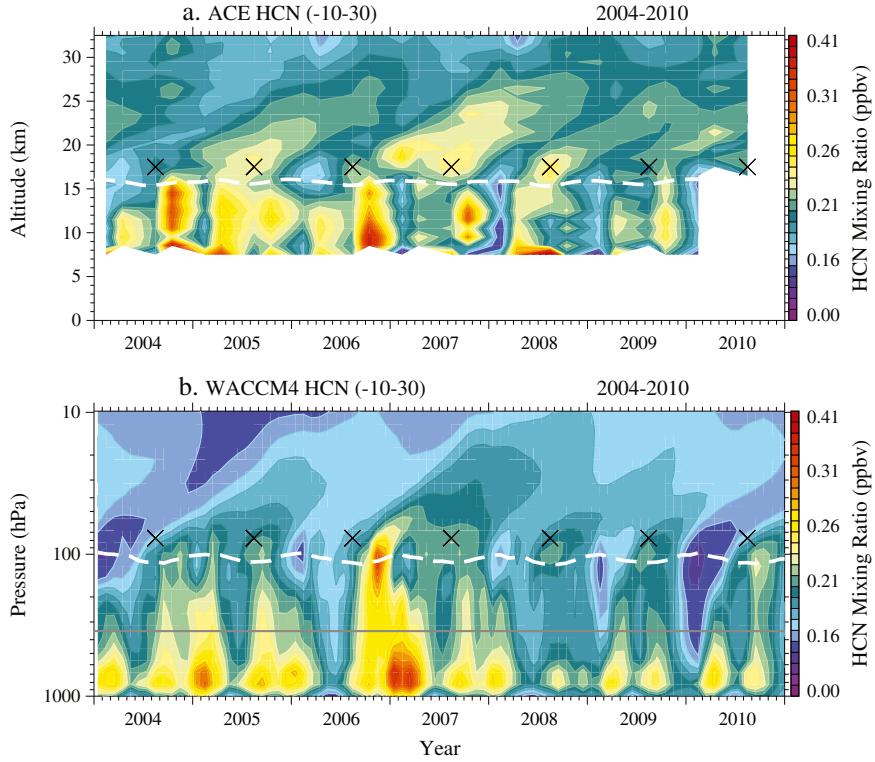

Figure 14. Time and altitude sections of zonally averaged HCN mixing ratios (ppbv) obtained from (a) ACE-FTS and (b) WACCM4 averaged over 10°S–30°N, respectively. White dashed line in Figure 14a denotes the tropopause obtained from NCEP/NCAR reanalysis and the one in Figure 14b represents the tropopause obtained from temperature profiles in WACCM4. August of each year is noted as a black cross near 18 km. Gray solid line in Figure 14b denotes approximate altitude of the lowest level of ACE-FTS HCN in Figure 14a.

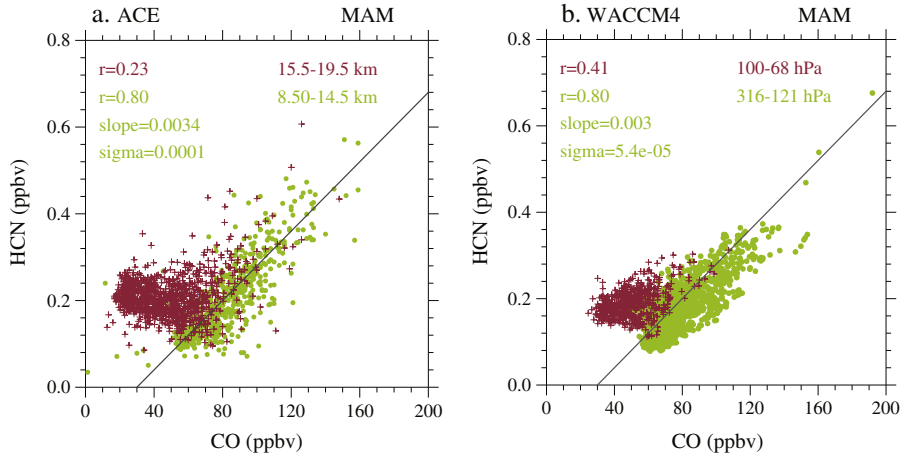

Figure 15. Same as Figure 10 but for HCN. The linear regression slope in Figure 15a (solid line) is calculated from the ACE-FTS measurements in the troposphere, and applied to WACCM4 in Figure 15b. Correlation coefficients calculated from stratospheric and tropospheric portions of the data are shown in the upper left corner in red and green, respectively. Linear regression slope and one sigma standard deviation of the tropospheric data are also shown in the upper left in green.

lifetimes and similar sources. The linear least square fit derived from ACE-FTS HCN vs. CO in the troposphere agrees well with the one from WACCM4 HCN vs. CO ($r = 0.80$). However, in the stratosphere the correlation is small ($r = 0.23$) because, unlike CO, the variability of HCN is not dominated by upward transport near the equator. The correlation between HCN vs. CO in WACCM4 (Figure 15b, sampled similarly to results in Figure 10) has similar behavior to ACE-FTS, reflecting the reasonable simulation of the different transport processes in WACCM4.

4. Summary and Discussion

[36] This study has focused on the global distributions and climatological seasonal behavior of several hydrocarbons observed by the ACE-FTS experiment, and on making detailed comparisons with the WACCM4 chemistry-climate model. While the ACE-FTS has limited space-time sampling, the overall behavior of seasonal average climatologies of CO derived from the multiyear ACE-FTS record (2004–2010) is found to agree reasonably well with results derived from MLS measurements for the same period (Figures 2–4). On the basis of agreement in CO from ACE-FTS and MLS, there is confidence in utilizing ACE-FTS data for additional species not measured by MLS. Variations of CO in the UTLS exhibit a well-known semiannual cycle in the tropics, linked to seasonal patterns in biomass burning and the semiannual cycle in low-latitude deep convection [*Jiang et al*., 2007; *Liu et al*., 2007], and there is an additional maximum in the NH summer tied to deep convection and transport in the Asian monsoon circulation [e.g., *Park et al*., 2009]. Variability above the tropical tropopause consists of an annual cycle with a maximum during NH winter/spring, tied to the strong annual cycle of tropical upwelling. Overall, WACCM4 is able to simulate much of the large-scale behavior for CO found in the observations, although the amount of CO in the SH subtropics during Austral spring is underestimated in the model.

[37] The behaviors of C_2H_6 and C_2H_2 closely follow the overall patterns of CO, and, as expected, there are strong correlations with CO in the individual ACE-FTS measurements (Figure 10). [*Rinsland et al*., 1998; *Zhao et al*., 2002; *Xiao et al*., 2007]. Because of its shorter photochemical lifetime, C_2H_2 exhibits stronger interhemispheric gradients than CO or C_2H_6. The WACCM4 simulation reproduces much of the observed structure and seasonality in C_2H_6 and C_2H_2, but the mixing ratios are consistently low compared to ACE-FTS. The most acute differences for both C_2H_6 and C_2H_2 occur in the SH subtropics during Austral spring, where it appears that the surface emissions or transport via deep convection in the model are underestimated.

[38] HCN exhibits behavior that is somewhat distinct from CO, C_2H_6, and C_2H_2 because (1) HCN has a much longer photochemical lifetime in the free atmosphere and (2) there is a substantial sink for HCN associated with contact with the ocean surface, so that a climatological minimum occurs in the UTLS over the tropical Pacific [*Randel et al*., 2010]. As a consequence of (1), gradients across the tropopause are weaker for HCN compared to the shorter-lived hydrocarbons. For HCN, the main pathway for transport to the stratosphere occurs through the Asian monsoon anticyclone during NH summer, which results in distinct behavior in the lower stratosphere compared to CO, C_2H_6, and C_2H_2 (or other species that are primarily transported to the stratosphere by upwelling in the deep tropics). HCN also shows substantial year-to-year variability, mainly influenced by enhanced biomass burning emissions linked to ENSO events (at least for the short ACE-FTS observational record). The WACCM4 simulation of HCN shows good agreement with the observations: the model is able to reproduce the key features of transport to the stratosphere through the Asian summer monsoon circulation and interannual variability linked to enhanced surface emissions. As with the other species, WACCM4 underestimates climatological HCN emissions in the SH subtropics during Austral spring.

[39] As discussed in the introduction, the behavior of hydrocarbons is important for key tropospheric chemical processes affecting tropospheric ozone and aerosols and their precursors, and accurate simulation of sources and large-scale transport are requisites for realistic tropospheric chemistry simulations. The ACE-FTS seasonal climatologies provide a unique high vertical resolution data set to constrain model behavior above the middle troposphere; we propose such data may be useful for standard model intercomparison studies. These gridded climatologies are available to the community via the web site (http://www.ace.uwaterloo.ca/) as supplementary material to this paper.

[40] **Acknowledgments.** We thank Steve Massie and Charles Bardeen for discussions and comments on the manuscript and three anonymous reviewers for constructive comments that improved the paper. This work was partially supported under the NASA Aura Science Program under grant NNX11AE59G. The ACE mission is funded primarily by the Canadian Space Agency. The National Center for Atmospheric Research is operated by the University Corporation for Atmospheric Research, under sponsorship of the National Science Foundation.

References

Abalos, M., W. J. Randel, and E. Serrano (2012), Variability in upwelling across the tropical tropopause and correlations with tracers in the lower stratosphere, *Atmos. Chem. Phys. Discuss.*, *12*, 18,817–18,851, doi:10.5194/acpd-12-18817-2012 DOI:10.5194%2Facpd-12-18817-2012.

Aikin, A. C., J. R. Herman, E. J. Maier, and C. J. McQuillan (1982), Atmospheric Chemistry of Ethane and Ethylene, *J. Geophys. Res.*, *87*, 3105–3118.

Akagi, S. K., R. J. Yokelson, C. Wiedinmyer, M. J. Alvarado, J. S. Reid, T. Karl, J. D. Crounse, and P. O. Wennberg (2011), Emission factors for open and domestic biomass burning for use in atmospheric models, *Atmos. Chem. Phys.*, *11*, 4039–4072, doi:10.5194/acp-11-4039-2011.

Baker, A. K., T. J. Schuck, F. Slemr, P. van Velthoven, A. Zahn, and C. A. M. Brenninkmeijer (2011), Characterization of non-methane hydrocarbons in Asian summer monsoon outflow observed by the CARIBIC aircraft, *Atmos. Chem. Phys.*, *11*, 503–518, doi:10.5194/acp-11-503-2011.

Barret, B., et al. (2008), Transport pathways of CO in the African upper troposphere during the monsoon season: a study based upon the assimilation of spaceborne observations, *Atmos. Chem. Phys.*, *8*, 3231–3246, doi:10.5194/acp-8-3231-2008.

Beer, R. (2006), TES on the aura mission: scientific objectives, measurements, and analysis overview, *IEEE Trans. Geosci. Remote Sensing*, *44*, 1102–1105, doi:10.1109/TGRS.2005.863716.

Bernath, P. F., et al. (2005), Atmospheric Chemistry Experiment (ACE): Mission overview, *Geophys. Res. Lett.*, *32*, L15S01, doi:10.1029/2005GL022386.

Bernath, P. F. (2006), Atmospheric Chemistry Experiment (ACE): Analytical chemistry from orbit, *Trends Anal. Chem.*, *25*(7), 647–654, doi:10.1016/j.trac.2006.05.001.

Boone, C. D., R. Nassar, K. A. Walker, Y. Rochon, S. D. McLeod, C. P. Rinsland, and P. F. Bernath (2005), Retrievals for the atmospheric chemistry experiment Fourier- transform spectrometer, *Appl. Opt.*, *44*, 7218–7231, doi:10.1364/AO.44.007218.

Bowman, K. P. (2006), Transport of carbon monoxide from the tropics to the extratropics, *J. Geophys. Res.*, *111*, D02107, doi:10.1029/2005JD006137.

Clerbaux, C., P.-F. Coheur, D. Hurtmans, B. Barret, M. Carleer, R. Colin, K. Semeniuk, J. C. McConnell, C. Boone, and P. Bernath (2005), Carbon monoxide distribution from the ACE-FTS solar occultation measurements, *Geophys. Res. Lett.*, *32*, L16S01, doi:10.1029/2005GL022394.

Clerbaux, C., et al. (2008), CO measurements from the ACE-FTS satellite instrument: data analysis and validation using ground-based, airborne and spaceborne observations, *Atmos. Chem. Phys.*, *8*, 2569–2594, doi:10.5194/acp-8-2569-2008.

Coheur, P.-F., et al. (2007), ACE-FTS observation of a young biomass burning plume: first reported measurements of C_2H_4, C_3H_6O, H_2CO and PAN by infrared occultation from space, *Atmos. Chem. Phys.*, *7*, 5437–5446, doi:10.5194/acp-7-5437-2007.

de Laat, A. T. J., A. M. S. Gloudemans, H. Schrijver, M. M. P. van den Broek, J. F. Meirink, I. Aben, and M. Krol (2006), Quantitative analysis

of SCIAMACHY carbon monoxide total column measurements, *Geophys. Res. Lett.*, *33*, L07807, doi:10.1029/2005GL025530.

De Smedt, I., T. Stavrakou, J.-F. Müller, R. J. van der A, and M. Van Roozendael (2010), Trend detection in satellite observations of formaldehyde tropospheric columns, *Geophys. Res. Lett.*, *37*, L18808, doi:10.1029/2010GL044245.

Dufour, G., C. D. Boone, C. P. Rinsland, and P. F. Bernath (2006), First space-borne measurements of methanol inside aged southern tropical to mid-latitude biomass burning plumes using the ACE-FTS instrument, *Atmos. Chem. Phys.*, *6*, 3463–3470, doi:10.5194/ acp-6-3463-2006 DOI:10.5194%2Facp-6-3463-2006.

Duncan, B. N., R. V. Martin, A. C. Staudt, R. Yevich, and J. A. Logan (2003), Interannual and seasonal variability of biomass burning emissions constrained by satellite observations, *J. Geophys. Res.*, *108*(D2), 4100, doi:10.1029/2002JD002378.

Duncan, B. N., J. A. Logan, I. Bey, I. A. Megretskaia, R. M. Yantosca, P. C. Novelli, N. B. Jones, and C. P. Rinsland (2007), Global budget of CO, 1988–1997: Source estimates and validation with a global model, *J. Geophys. Res.*, *112*, D22301, doi:10.1029/2007JD008459.

Edwards, D. P., et al. (2004), Observations of carbon monoxide and aerosols from the Terra satellite: Northern Hemisphere variability, *J. Geophys. Res.*, *109*, D24202, doi:10.1029/2004JD004727.

Edwards, D. P., et al. (2006), Satellite-observed pollution from Southern Hemisphere biomass burning, *J. Geophys. Res.*, *111*, D14312, doi:10.1029/2005JD006655.

Emmons, L. K., et al. (2010), Description and evaluation of the Model for Ozone and Related chemical Tracers, version 4 (MOZART-4), *Geosci. Model Dev.*, *3*, 43–67, doi:10.5194/gmd-3-43-2010.

Fischer, H., et al. (2008), MIPAS: an instrument for atmospheric and climate research, *Atmos. Chem. Phys.*, *8*, 2151–2188, doi:10.5194/ acp-8-2151-2008 DOI:10.5194%2Facp-8-2151-2008.

Funke, B. M., et al. (2009), Carbon monoxide distributions from the upper troposphere to the mesosphere inferred from 4.7μm non-local thermal equilibrium emissions measured by MIPAS on Envisat, *Atmos. Chem. Phys.*, *9*, 2387–2411.

Garcia, R. R., D. R. Marsh, D. E. Kinnison, B. A. Boville, and F. Sassi (2007), Simulation of secular trends in the middle atmosphere, 1950–2003, *J. Geophys. Res.*, *112*, D09301, doi:10.1029/2006JD007485.

George, M., et al. (2009), Carbon monoxide distributions from the IASI/ METOP mission: evaluation with other space-borne remote sensors, *Atmos. Chem. Phys.*, *9*, 8317–8330, doi:10.5194/acp-9-8317-2009 DOI:10.5194%2Facp-9-8317-2009 .

Glatthor, N., T. von Clarmann, G. P. Stiller, B. Funke, M. E. Koukouli, H. Fischer, U. Grabowski, M. Höpfner, S. Kellmann, and A. Linden (2009), Large-scale upper tropospheric pollution observed by MIPAS HCN and C_2H_6 global distributions, *Atmos. Chem. Phys.*, *9*, 9619–9634, doi:10.5194/acp-9-9619-2009.

González Abad, G., et al. (2011), Ethane, ethyne and carbon monoxide concentrations in the upper troposphere and lower stratosphere from ACE and GEOS-Chem: a comparison study, *Atmos. Chem. Phys.*, *11*, 9927–9941, doi:10.5194/acp-11-9927-2011.

Granier et al. (2005), POET, a database of surface emissions of ozone precursors. [http://www.aero.jussieu.fr/projet/ACCENT/POET.php.]

Guenther, A., T. Karl, P. Harley, C. Wiedinmyer, P. I. Palmer, and C. Geron (2006), Estimates of global terrestrial isoprene emissions using MEGAN (Model of Emissions of Gases and Aerosols from Nature), *Atmos. Chem. Phys.*, *6*, 3181–3210, doi:10.5194/acp-6-3181-2006.

Guenther, A. B., X. Jiang, C. L. Heald, T. Sakulyanontvittaya, T. Duhl, L. K. Emmons, and X. Wang (2012), The Model of Emissions of Gases and Aerosols from Nature version 2.1 (MEGAN2.1): an extended and updated framework for modeling biogenic emissions, *Geosci. Model Dev.*, *5*, 1471–1492, doi:10.5194/gmd-5-1471-2012.

Hegglin, M. I., C. D. Boone, G. L. Manney, and K. A. Walker (2009), A global view of the extratropical tropopause transition layer from Atmospheric Chemistry Experiment Fourier Transform Spectrometer O_3, H_2O, and CO, *J. Geophys. Res.*, *114*, D00B11, doi:10.1029/2008JD009984.

Jiang, J. H., N. J. Livesey, H. Su, L. Neary, J. C. McConnell, and N. A. D. Richards (2007), Connecting surface emissions, convective uplifting, and long-range transport of carbon monoxide in the upper troposphere: New observations from the Aura Microwave Limb Sounder, *Geophys. Res. Lett.*, *34*, L18812, doi:10.1029/2007GL030638.

Kinnison, D. E., et al. (2007), Sensitivity of chemical tracers to meteorological parameters in the MOZART-3 chemical transport model, *J. Geophys. Res.*, *112*, D20302, doi:10.1029/2006JD007879.

Kistler, R., et al. (2001), The NCEP/NCAR 50-year reanalysis: Monthly means CD-ROM and documentation, *Bull. Am. Met. Soc.*, *82*, 247–267.

Kleinböhl, A., G. C. Toon, B. Sen, J. -F. L. Blavier, D. K. Weisenstein, R. S. Strekowski, J. M. Nicovich, P. H. Wine, and P. O. Wennberg (2006), On the stratospheric chemistry of hydrogen cyanide, *Geophys. Res. Lett.*, *33*, L11806, doi:10.1029/2006GL026015.

Kopacz, M., et al. (2010), Global estimates of CO sources with high resolution by adjoint inversion of multiple satellite datasets (MOPITT, AIRS, SCIAMACHY, TES), *Atmos. Chem. Phys.*, *10*, 855–876, doi:10.5194/ acp-10-855-2010.

Kunz, A., L. L. Pan, P. Konopka, D. E. Kinnison, and S. Tilmes (2011), Chemical and dynamical discontinuity at the extratropical tropopause based on START08 and WACCM analyses, *J. Geophys. Res.*, *116*, D24302, doi:10.1029/2011JD016686.

Lamarque, J.-F., et al. (2012), CAM-chem: description and evaluation of interactive atmospheric chemistry in CESM, *Geosci. Model Dev.*, *5*, 369–411, doi:10.5194/gmd-5-369-2012.

Lamarque, J. -F., et al. (2010), Historical (1850–2000) gridded anthropogenic and biomass burning emissions of reactive gases and aerosols: methodology and application, *Atmos. Chem. Phys.*, *10*, 7017–7039, doi:10.5194/acp-10-7017-2010.

Li, Q., et al. (2003), A global three-dimensional model analysis of the atmospheric budgets of HCN and CH_3CN: Constraints from aircraft and ground measurements, *J. Geophys. Res.*, *108*(D21), 8827, doi:10.1029/ 2002JD003075.

Li, Q., et al. (2005), Convective outflow of South Asian pollution: A global CTM simulation compared with EOS MLS observations, *Geophys. Res. Lett.*, *32*, L14826, doi:10.1029/2005GL022762.

Li, Q., P. I. Palmer, H. C. Pumphrey, P. Bernath, and E. Mahieu (2009), What drives the observed variability of HCN in the troposphere and lower stratosphere? *Atmos. Chem. Phys.*, *9*, 8531–8543, doi:10.5194/ acp-9-8531-2009 DOI:10.5194%2Facp-9-8531-2009.

Liebman, B., and C. A. Smith (1996), Description of a complete (interpolated) outgoing longwave radiation dataset, *Bull. Am. Meteorol. Soc.*, *77*, 1275–1277.

Lin, S.-J. (2004), A "vertically-Lagrangian" finite-volume dynamical core for global atmospheric models, *Mon. Wea. Rev.*, *132*, 2293–2307, doi:10.1175/1520-0493(2004)132<2293:AVLFDC>2.0.CO;2.

Liu, C., E. Zipser, T. Garrett, J. H. Jiang, and H. Su (2007), How do the water vapor and carbon monoxide "tape recorders" start near the tropical tropopause?, *Geophys. Res. Lett.*, *34*, L09804, doi:10.1029/2006GL029234.

Liu, J., J. A. Logan, D. B. A. Jones, N. J. Livesey, I. A. Megretskaia, C. C. Carouge, and P. Nedelec (2010), Analysis of CO in the tropical troposphere using Aura satellite data and the GEOS-Chem model: insights into transport characteristics of the GEOS meteorological products, *Atmos. Chem. Phys.*, *10*, 12,207–12,232, doi:10.5194/acp-10-12207-2010.

Livesey, N. J., et al. (2008), Validation of Aura Microwave Limb Sounder O_3 and CO observations in the upper troposphere and lower stratosphere, *J. Geophys. Res.*, *113*, D15S02, doi:10.1029/2007JD008805.

Livesey, N. J., et al. (2011), Earth Observing System (EOS) Aura Microwave Limb Sounder (MLS) version 3.3 level 2 data quality and description document, *JPL D-33509*, Jet Propulsion Laboratory, California Institute of Technology, Pasadena, California, USA, 162 pp.

Logan, J. A., I. A. Megretskaia, R. Nassar, L. T. Murray, L. Zhang, K. W. Bowman, H. M. Worden, and M. Luo (2008), Effects of the 2006 El Nino on tropospheric composition as revealed by data from the Tropospheric Emission Spectrometer (TES), *Geophys. Res. Lett.*, *35*, L03816, doi:10.0129GL031698.

Luo, M., et al. (2007), TES carbon monoxide validation with DACOM aircraft measurements during INTEX-B 2006, *J. Geophys. Res.*, *112*, D24S48, doi:10.1029/2007JD008803.

Lupu, A., et al. (2009), Hydrogen cyanide in the upper troposphere: GEM-AQ simulation and comparison with ACE-FTS observations, *Atmos. Chem. Phys.*, *9*, 4301–4313, doi:10.5194/acp-9-4301-2009.

Marcy, T. P., et al. (2004), Quantifying stratospheric ozone in the upper troposphere with in situ measurements of HCl, *Science*, *304*, 261–265, doi:10.1126/science.1093418.

Ohara, T., H. Akimoto, J. Kurokawa, N. Horii, K. Yamaji, X. Yan, and T. Hayasaka (2007), An Asian emission inventory of an-thropogenic emission sources for the period 1980-2020, *Atmos. Chem. Phys.*, *7*, 4419–4444.

Pan, L. L., W. J. Randel, B. L. Gary, M. J. Mahoney, and E. J. Hintsa (2004), Definitions and sharpness of the extratropical tropopause: A trace gas perspective, *J. Geophys. Res.*, *109*, D23103, doi:10.1029/ 2004JD004982.

Park, M., W. J. Randel, A. Gettelman, S. T. Massie, and J. H. Jiang (2007), Transport above the Asian summer monsoon anticyclone inferred from Aura Microwave Limb Sounder tracers, *J. Geophys. Res.*, *112*, D16309, doi:10.1029/2006JD008294.

Park, M., W. J. Randel, L. K. Emmons, P. F. Bernath, K. A. Walker, and C. D. Boone (2008), Chemical isolation in the Asian monsoon anticyclone observed in Atmospheric Chemistry Experiment (ACE-FTS) data, *Atmos. Chem. Phys.*, *8*, 757–764, doi:10.5194/ acp-8-757-2008 DOI:10.5194% 2Facp-8-757-2008.

Park, M., W. J. Randel, L. K. Emmons, and N. J. Livesey (2009), Transport pathways of carbon monoxide in the Asian summer monsoon diagnosed

from Model of Ozone and Related Tracers (MOZART), *J. Geophys. Res.*, *114*, D08303, doi:10.1029/2008JD010621.

Parker, R. J., J. J. Remedios, D. P. Moore, and V. P. Kanawade (2011), Acetylene C_2H_2 retrievals from MIPAS data and regions of enhanced upper tropospheric concentrations in August 2003, *Atmos. Chem. Phys.*, *11*, 10,243–10,257, doi:10.5194/acp-11-10243-2011.

Pickering, K., et al. (1996), Convective transport of biomass burning emissions over Brazil during TRACE A, *J. Geophys. Res.*, *101*(D19), 23,993–24,012.

Pommrich, R. et al. (2010), What causes the irregular cycle of the atmospheric tape recorder signal in HCN? *Geophys. Res. Lett.*, *37*, L16805, doi:10.1029/2010GL044056.

Pumphrey, H. C., C. Boone, K. A. Walker, P. Bernath, and N. J. Livesey (2008), Tropical tape recorder observed in HCN, *Geophys. Res. Lett.*, *35*, L05801, doi:10.1029/ 2007GL032137.

Randel, W. J., and M. Park (2006), Deep convective influence on the Asian summer monsoon anticyclone and associated tracer variability observed with Atmospheric Infrared Sounder (AIRS), *J. Geophys. Res.*, *111*, D12314, doi:10.1029/2005JD006490.

Randel, W. J., M. Park, F. Wu, N. Livesey (2007), A large annual cycle in ozone above the tropical tropopause linked to the Brewer–Dobson circulation, *J. Atmos. Sci.*, *64*, 4479–4488, doi: 10.1175/2007JAS2409.1.

Randel, W. J., M. Park, L. Emmons, D. Kinnison, P. Bernath, K. Walker, C. Boone and H. Pumphrey (2010), Asian monsoon transport of pollution to the stratosphere, *Science*, *328*, 611–613, doi:10.1126/ science.1182274.

Rienecker, M. M., et al. (2011), MERRA - NASA's Modern-Era Retrospective Analysis for Research and Applications. *J. Climate*, *24*, 3624–3648, doi:10.1175/JCLI-D-11-00015.1.

Rinsland, C., et al. (1998), Northern and southern hemisphere ground-based infrared spectroscopic measurements of tropospheric carbon monoxide and ethane, *J. Geophys. Res.*, *103*(D21), 28,197–28,217.

Rinsland, C. P., G. Dufour, C. D. Boone, P. F. Bernath, and L. Chiou (2005), Atmospheric Chemistry Experiment (ACE) measurements of elevated Southern Hemisphere upper tropospheric CO, C_2H_6, HCN, and C_2H_2 mixing ratios from biomass burning emissions and long-range transport, *Geophys. Res. Lett.*, *32*, L20803, doi:10.1029/2005GL024214.

Rinsland, C. P., G. Dufour, C. D. Boone, P. F. Bernath, L. Chiou, P.-F. Coheur, S. Turquety, and C. Clerbaux (2007), Satellite boreal measurements over Alaska and Canada during June–July 2004: Simultaneous measurements of upper tropospheric CO, C_2H_6, HCN, CH_3Cl, CH_4, C_2H_2, CH_3OH, HCOOH, OCS, and SF_6 mixing ratios, *Global Biogeochem. Cycles*, *21*, GB3008, doi:10.1029/2006GB002795.

Rudolph, J. (1995), The tropospheric distribution and budget of ethane, *J. Geophys. Res.*, *100*(D6), 11,369–11,381.

Russo, R., et al. (2003), Chemical composition of Asian continental outflow over the western Pacific: Results from Transport and Chemical Evolution over the Pacific (TRACE-P), *J. Geophys. Res.*, *108*(D20), 8804–8823, doi:10.1029/2002JD003184.

Sander et al. (2006), Chemical Kinetics and Photochemical Data for Use in Atmospheric Studies - Evaluation Number 15, *JPL Publication 06-2*, Jet Propulsion Laboratory. [http://jpldataeval.jpl.nasa.gov.]

Schneider, J., V. Bürger, and F. Arnold (1997), Methyl cyanide and hydrogen cyanide measurements in the lower stratosphere: Implications for methyl cyanide sources and sinks, *J. Geophys. Res.*, *102*, 25,501–25,506.

Shindell, D. T., et al. (2006), Multimodel simulations of carbon monoxide: Comparison with observations and projected near-future changes, *J. Geophys. Res.*, *111*, D19306, doi:10.1029/2006JD007100.

Singh, H. B., et al. (2003), In situ measurements of HCN and CH_3CN over the Pacific Ocean: Sources, sinks, and budgets, *J. Geophys. Res.*, *108* (D20), 8795–8809, doi:10.1029/ 2002JD003006.

Taguchi, M. (2009), Wave driving in the tropical lower stratosphere as simulated by WACCM. Part I: Annual cycle, *J. Atmos. Sci.*, *66*, 2029–2043, doi:10.1175/2009JAS2854.1.

Tereszchuk, K. A., G. González Abad, C. Clerbaux, D. Hurtmans, P.-F. Coheur, and P. F. Bernath (2011), ACE-FTS measurements of trace species in the characterization of biomass burning plumes, *Atmos. Chem. Phys.*, *11*, 12,169–12,179, doi:10.5194/acp-11-12169-2011.

Tilmes, S., et al. (2010), An aircraft-based upper troposphere lower stratosphere O_3, CO, and H_2O climatology for the Northern Hemisphere, *J. Geophys. Res.*, *115*, D14303, doi:10.1029/2009JD012731.

Turquety, S., et al. (2008), CO emission and export from Asia: an analysis combining complementary satellite measurements (MOPITT, SCIAMACHY and ACE-FTS) with global modeling, *Atmos. Chem. Phys.*, *8*, 5187–5204, doi:10.5194/acp-8-5187-2008 DOI:10.5194%2Facp-8-5187-2008.

Turquety, S., D. Hurtmans, J. Hadji-Lazaro, P.-F. Coheur, C. Clerbaux, D. Josset, and C. Tsamalis (2009), Tracking the emission and transport of pollution from wildfires using the IASI CO retrievals: analysis of the summer 2007 Greek fires, *Atmos. Chem. Phys.*, *9*, 4897–4913, doi:10.5194/acp-9-4897-2009 DOI:10.5194%2Facp-9-4897-2009.

van der Werf, G. R., J. T. Randerson, L. Giglio, G. J. Collatz, M. Mu, P. S. Kasibhatla, D. C. Morton, R. S. DeFries, Y. Jin, and T. T. van Leeuwen (2010), Global fire emissions and the contribution of deforestation, savanna, forest, agricultural, and peat fires (1997–2009), *Atmos. Chem. Phys.*, *10*, 11,707–11,735, doi:10.5194/acp-10-11707-2010.

von Clarmann, T., N. Glatthor, M. E. Koukouli, G. P. Stiller, B. Funke, U. Grabowski, M. H. Öpfner, S. Kellmann, A. Linden, M. Milz, T. Steck, and H. Fischer (2007), MIPAS measurements of upper tropospheric C_2H_6 and O_3 during the southern hemispheric biomass burning season in 2003, *Atmos. Chem. Phys.*, *7*, 5861–5872, doi:10.5194/acp-7-5861-2007.

Waters, J. W., et al. (2006), The Earth Observing System Microwave Limb Sounder (EOS MLS) on the Aura satellite, *IEEE Trans. Geosci. Remote Sens.*, *44*(5), 1075–1092, doi:10.1109/ TGRS.2006.873771 DOI:10.1109%2FTGRS.2006.873771.

Wiegele, A., N. Glatthor, M. Höpfner, U. Grabowski, S. Kellmann, A. Linden, G. Stiller, and T. von Clarmann (2012), Global distributions of C_2H_6, C_2H_2, HCN, and PAN retrieved from MIPAS reduced spectral resolution measurements, *Atmos. Meas. Tech.*, *5*, 723–734, doi:10.5194/amt-5-723-2012.

Xiao Y., D. J. Jacob, S. Turquety (2007), Atmospheric acetylene and its relationship with CO as an indicator of air mass age, *J. Geophys. Res.*, *112*, D12305, doi:10.1029/2006JD008268.

Xiao, Y., J. A. Logan, D. J. Jacob, R. C. Hudman, R. Yantosca, and D. R. Blake (2008), Global budget of ethane and regional constraints on U.S. sources, *J. Geophys. Res.*, *113*, D21306, doi:10.1029/2007JD009415.

Zhang, L., et al. (2011), Impacts of 2006 Indonesian fires and dynamics on tropical upper tropospheric carbon monoxide and ozone, *Atmos. Chem. Phys.*, *11*, 10,929–10,946, doi:10.5194/acp-11-10929-2011.

Zhao, Y., et al. (2002), Spectroscopic measurements of tropospheric CO, C_2H_6, C_2H_2, and HCN in northern Japan, *J. Geophys. Res.*, *107*(D18), 4343–4359, doi:10.1029/2001JD000748.